Drafting the CLN3 protein interactome in SH-SY5Y human neuroblastoma cells: a label-free quantitative proteomics approach.

Enzo Scifo[1,10*], Agnieszka Szwajda[2], Janusz Dńbski[3], Kristiina Uusi-Rauva[4,9], Tapio Kesti[5], Michaŭ Dadlez[3], Anne-Claude Gingras[6], Jaana Tyynelä[7], Marc H. Baumann[7], Anu Jalanko[8,9] and Maciej Lalowski[4,7*].

[1]Meilahti Clinical Proteomics Core Facility, Institute of Biomedicine / Anatomy, University of Helsinki, Helsinki, Finland
[2]Institute for Molecular Medicine (FIMM), University of Helsinki, Helsinki, Finland
[3]Mass Spectrometry Laboratory, Department of Biophysics, Institute of Biochemistry and Biophysics, Polish Academy of Sciences, Warsaw, Poland
[4]Folkhälsan Institute of Genetics, Helsinki, Finland
[5]Department of Virology, Haartman Institute, University of Helsinki and Helsinki University Central Hospital, Helsinki, Finland
[6]Centre for Systems Biology, Samuel Lunenfeld Research Institute at Mount Sinai Hospital, Toronto, and Department of Molecular Genetics, University of Toronto, Ontario, Canada
[7]Meilahti Clinical Proteomics Core Facility, Institute of Biomedicine / Biochemistry and Developmental Biology, University of Helsinki, Helsinki, Finland
[8]Public Health Genomics Unit, Department of Chronic Disease Prevention, Helsinki, Finland
[9]National Institute for Health and Welfare, Helsinki, Finland
[10]Finnish Graduate School of Neuroscience, University of Helsinki, Helsinki, Finland

[*]Address correspondence to:
Dr. Maciej Lalowski, Biomedicum Helsinki, Meilahti Clinical Proteomics Core Facility, P.O Box 63 (Haartmaninkatu 8), Room C214a, FI-00014 University of Helsinki, Finland, Tel. +358-9-19125203, Fax +358-9-19125206, E-Mail: maciej.lalowski@helsinki.fi

Enzo Scifo, Biomedicum Helsinki, Meilahti Clinical Proteomics Core Facility, P.O Box 63 (Haartmaninkatu 8), Room C217, FI-00014 University of Helsinki, Finland, Tel. +358-9-19125202, Fax +358-9-19125206, E-Mail: enzo.scifo@helsinki.fi

Abbreviations: CLN3/5/6, Ceroid-lipofuscinosis neuronal protein 3/5/6; CTAP-Puro, Expression plasmid pES-CTAP-Puro; ERAD, Endoplasmic-reticulum-associated protein degradation; FDR, False discovery rate; GFP, Green fluorescent protein; GO, Gene ontology; Gw, Gateway; HCIP, High confidence Interacting partners; HEK 293, Human embryonic kidney 293; IF, Immunofluorescence; IP, Interacting partners; JNCL, Juvenile neuronal ceroid lipofuscinosis; LTQ, Linear trap quadrupole; NCL, Neuronal ceroid lipofuscinoses; NTAP, Expression plasmid pCeMM-NTAP(GS)Gw; PA, Protein A; PPI, Protein-Protein interactions; RNase A; Ribonuclease A; SAINT, Significance Analysis of INTeractome; SBP, Streptavidin binding peptide; TAP-MS, Tandem affinity purification coupled to mass spectrometry; TCEP, Tris-carboxyethyl-phosphine; TEV, Tobacco etch virus; Y2H, Yeast two hybrid

Keywords:

Neuronal ceroid lipofuscinoses, CLN3 disease, Interactome, Tandem Affinity Purification, Mass Spectrometry, Co-immunoprecipitation

ABSTRACT

Neuronal ceroid lipofuscinoses (NCL) are the most common inherited progressive encephalopathies of childhood. One of the most prevalent forms of NCL, Juvenile neuronal ceroid lipofuscinosis (JNCL) or CLN3 disease (OMIM: 204200) is caused by mutations in the *CLN3* gene on chromosome 16p12.1. Despite progress in the NCL field, the primary function of ceroid-lipofuscinosis neuronal protein 3 (CLN3) remains elusive. In this study, we aimed to clarify the role of human CLN3 in the brain by identifying CLN3-associated proteins using a Tandem Affinity Purification coupled to Mass Spectrometry (TAP-MS) strategy combined with Significance Analysis of INTeractome (SAINT). Human SH-SY5Y-NTAP-CLN3 stable cells were used to isolate native protein complexes for subsequent TAP-MS. Bioinformatic analyses of isolated complexes, yielded: 58 CLN3 interacting partners (IP) including 42 novel CLN3 IP, as well as 16 CLN3 high confidence interacting partners (HCIP) previously identified in another high-throughput study by Behrends et al., 2010. Moreover, 31 IP of ceroid-lipofuscinosis neuronal protein 5 (CLN5), were identified (18 of which were in common with the CLN3 bait). Our findings support previously suggested involvement of CLN3 in transmembrane transport, lipid homeostasis and neuronal excitability, as well as link it to G-protein signalling and protein folding / sorting in the ER.

1. INTRODUCTION

Proteins rarely function in isolation but rather as macromolecular complexes that orchestrate cellular processes. Moreover, protein complexes are dynamic entities with spatial and temporal variation in composition, depending on their cellular environment [1]. Consequently, and through implication by association, the function and cellular localisation of previously characterised interactors of a protein will inform on its function, pathway and localisation within the cell. Particularly, the design of protein interaction networks offers clues about disease processes or mechanisms of action, which may be exploited for therapeutic applications.

Yeast two hybrid (Y2H) and tandem affinity purification coupled to mass spectrometry (TAP-MS) are the two most widely used experimental techniques to measure protein-protein interactions (PPI) [2-7]. Both have been used to generate large-scale PPI networks for human [5-10] and several model organisms including *C. elegans* [11, 12], *D. melanogaster* [13, 14] and *S. cerevisiae* [3, 15]. Although, Y2H technology is the most standardised technique in identifying and mapping PPI, it requires stringent criteria for screening and rigorous validation of hits [6, 7]. In contrast, TAP-MS is an efficient and gentle method to isolate protein complexes from cells at near to physiological levels [16, 17]. It is however biased towards proteins that bind with high affinity and have slow kinetics of dissociation [18]. PPI obtained from Y2H or TAP-MS are typically further validated by several biochemical, genetic or physical methods, in an effort to increase confidence in the dataset [18]. The various methods for mapping PPI generate complementary rather than overlapping data [19, 20].

Neuronal ceroid lipofuscinoses (NCL) are characterised by early accumulation of auto-fluorescent storage material in lysosomes of neurons or other cells and degeneration of cortical neurons. Clinically, NCL patients suffer from progressive loss of vision, mental and

motor deterioration, epileptic seizures and premature death [21]. NCL are caused by nearly 400 mutations (mostly autosomal recessively inherited) in thirteen known genes (*CLN1-8*, *CLN10-14*; http://www.ucl.ac.uk/ncl) and have an estimated incidence of 1 case per 12,500-200,000 persons, in the USA and Northern Europe [21, 22]. Mutations in the *CLN3* gene, which encodes a hydrophobic integral membrane protein of 438 amino acids, are known to cause Juvenile neuronal ceroid lipofuscinosis (JNCL) or CLN3 disease (OMIM: 204200) [21, 23]. CLN3 disease is the most common of all NCL [23, 24]. In neurons, the CLN3 protein is primarily localised in endosomes / lysosomes and transported to synaptosomes [24].

Despite extensive efforts to elucidate the functions of CLN3 using several models such as yeast, mammalian cells, mouse, and *Drosophila* [8, 25-42], there is still no consensus on the function of CLN3. Recently, CLN3 was shown to interact with Rab7 and RILP [41], whereas earlier studies reported CLN3 interactions with: myosin IIB [28], Shwachman-Bodian Diamond-Syndrome (SBDS) [42], ß-fodrin and Na^+-K^+-ATPase complex [40], calsenilin [26], and Hook1 [33]. Experiments in yeast (*S. cerevisiae and S. pombe*) implicated CLN3 in endosome-Golgi-retrograde transport [31], vacuole protein sorting [27], vacuolar pH homeostasis and arginine transport [32, 36]. Moreover, investigations in mammalian cells and mouse models showed involvement of CLN3 in intracellular trafficking [33, 34, 41], lipid metabolism [30, 35], galactosyl-ceramide transport [38], sphingolipid homeostasis [38], autophagy [8, 25], lysosomal arginine transport [37], pH homeostasis [29], and apoptosis [43].

Thus far, a majority of PPI networks generated using affinity tagging and mass spectrometry in mammalian cells, were established in cancer cell lines of non-neuronal lineage. However, in a few recent publications (generation of muscarinic receptors interactome or identification of binding partners of clustered protocadherins in the nervous system) cells of neuronal origin have been utilised [44, 45]. To gain further insight into the

mechanistic and biological functions of human CLN3 in the brain, we mapped its protein interaction network in human neuroblastoma cells. Our approach involved generation of SH-SY5Y-NTAP-CLN3 stable cells, which were processed and analysed by TAP-MS. We used a recently developed Significance Analysis of INTeractome (SAINT) algorithm [46] that relies on statistical analysis of spectral count distributions to discern true interactions from false ones. Based on this statistical platform, we identified 58 CLN3 interacting partners (IP), including 42 novel CLN3 IP. Our data confirm previously reported interactions of CLN3 with Na+/K+ ATPase [40], IMMT, GCN1L1, PRKDC, XPO1, CPT1A, HSD17B12, RPN2, PHGDH, COX15, SLC25A11, DDOST, AUP1, KIAA0368, SLC25A22, SLC25A10 and NUP205 [8]. Functional annotation using Gene Ontology (GO)_biological process of the CLN3 IP by Database for Annotation, Visualization and Integrated Discovery (DAVID, http://david.abcc.ncifcrf.gov/tools.jsp) [47] software, revealed known CLN3-associated functional modules (transmembrane transport, lipid biosynthetic process and nitrogen compound biosynthetic process) and a novel one, generation of precursor metabolites and energy.

2. EXPERIMENTAL PROCEDURES

2.1. DNA expression constructs

Full length CLN3 (IOH3475) and CLN5 (OCABo5050F1210) entry clones purchased from Source BioScience UK Limited (Nottingham, UK), were shuttled in pCeMM-NTAP(GS)-Gw (NTAP) [48] and pES-CTAP-Puro (CTAP-Puro, Supplementary Material), respectively, for TAP-MS experiments. Recombination of DNA fragments was performed using the LR clonase reaction (Life Technologies Europe BV, Espoo, Finland) and analysed with BsrGI restriction enzyme. Full length entry clones for co-immunoprecipitation experiments: CLN3 (IOH3475), DBH (OCAAo5051B0535D), DPM1 (IOH7445) and SEC61A1

(OCABo5050C1119D) were purchased from Source BioScience UK Limited; SLC25A10 (RZPDo839F08152), SLC25A11 (RZPDo839G0296) and SLC25A22 (RZPDo839E0876) were kind gifts from Prof. Erich Wanker (MDC, Berlin). They were shuttled into pcDNA3.1/nV5-Dest (Life Technologies Europe BV), pcDNA3.1-ProtA-D57 (E. Wanker) Gateway vectors and similarly processed as indicated above.

2.2. Retroviral production, transduction and generation of stable cell lines

For producing retroviral particles, DNA of retroviral vectors was introduced into HEK 293T cells [49, 50] simultaneously with two packaging plasmids: pCMV-Gag-Pol vector (expresses gag protein and reverse transcriptase of Moloney murine leukemia virus) [51] and pVSV-G (expresses protein G of vesicular stomatitis virus) [52]. The three plasmids were mixed in proportions of 7.5:5:1, respectively and introduced into cells using the calcium phosphate method according to the manufacturer's protocol (Life Technologies Europe BV). Cell-free virus was harvested two days post transfection, filtered through 0.45 εm pore size filter (Millex-HV Filter Unit, Millipore, Ireland Ltd) and used to infect low passage (P5-10) SH-SY5Y cells. Cells were grown in DMEM: F12 Ham's media (1:1), supplemented with Penicillin (100 µg/ml), Streptomycin (100 µg/ml), Glutamine, non-essential amino acids (1x) and 10% FBS (Life Technologies Europe BV), at 37°C under humidified atmosphere of 95% air and 5% CO_2. Stable integrants were selected by sorting GFP positive cells using flow cytometry and confirmed with immunocytochemistry and Western blot analysis (see section 2.4 and Supplementary Material). Stably infected cells were maintained in an undifferentiated state (Ò 80% confluence) and constantly checked for consistent growth rates and morphological features.

2.3. Cell culture, transfection and co-immunoprecipitation assay

HEK 293 cells were maintained in DMEM, supplemented with Penicillin (100 µg/ml), Streptomycin (100 µg/ml), Glutamine and 10% FBS, at 37°C under humidified atmosphere of 95% air and 5% CO_2. Pairs of V5-CLN3 IP and PA-CLN3 tagged constructs (or vice versa) were transiently co-transfected in HEK-293 cells in 24 well plate format, using Fugene HD transfection reagent (Roche Diagnostics Oy, Espoo, Finland) according to the manufacturer's instructions. After 48 h, transfected cells were harvested with lysis buffer (50 mM HEPES, pH 7.4, 150 mM NaCl, 1 mM EDTA, 1% Nonidet P-40, 1 mM DTT and 10% glycerol) supplemented with benzonase (E1014, 250U), protease inhibitors: 1 mM PMSF (P7626; Sigma-Aldrich Finland Oy, Helsinki, Finland) and 1 x protease inhibitor cocktail (Cat. No. 04693116001, Roche Diagnostics Oy), for 30 min. Handling and processing of samples was done at 4°C. Cytoplasmic extracts were analysed by SDS-PAGE to control for uniform gene expression profiles, prior to isolation of protein complexes from 100 µl cell extracts incubated with shaking on 10 µl Dynabeads M-280 Sheep anti-Rabbit IgG (11204D; Life Technologies Europe BV), for 1 h. Bound beads were washed thrice with 100 µl minimum lysis buffer, resuspended in 25 µl PBS and an equal volume of 2x sample loading buffer. Mouse monoclonal anti-V5 (R960-25; 1:5,000, Life Technologies Europe BV) was used to probe for co-immunoprecipitation with CLN3.

2.4. Western Blotting and Antibodies

Primary antibodies used were: rabbit polyclonal anti-CLN3 (ab75959, 1:700), mouse monoclonal anti-Myc [9E10] (ab32, 1:1000), and mouse monoclonal anti-LAMP 1 [H4A3] (ab25630, 1:300) (Abcam plc, Cambridge, UK); rabbit polyclonal anti-CLN5 [C/32] (1:500) [53]; mouse monoclonal anti-V5 (R960-25, 1:5,000; Life Technologies Europe BV);

rabbit polyclonal anti-PA (5500-100; 1:10,000, Biovision, Germany); and mouse monoclonal anti-ϐ-actin [AC15] (A1978, 1:1000) (Sigma-Aldrich Finland Oy). Each antibody was used according to the manufacturer's protocols.

2.5. TAP tag purification

Monolayer cells were harvested from five 150 mm plates of NTAP-CLN3 or CLN5-CTAP-IRES-Puro infected SH-SY5Y cells, grown to 80% confluency (1×10^8 cells). Cells were washed thrice with ice cold 1x PBS, flash frozen and lysed in 5ml Lysis buffer (50 mm HEPES, pH 7.4, 150 mM NaCl, 1 mM EDTA, 1% Nonidet P-40, and 10% glycerol) supplemented with benzonase nuclease (250U, E1014) and protease inhibitors (1 mM PMSF and 1x protease inhibitor cocktail), for 30 min at 4°C. Cytoplasmic extraction from the cell lysates was done by centrifugation at maximum speed (18,000 rpm) for 10 min., thereby pelleting cell nuclei. The supernatant was used for batch purification of the IgG binding domain (TAP)-tagged protein complexes using 200 εl of packed IgG-Sepharose 6 Fast Flow resin (Amersham Biosciences). Lysates were incubated with resin for 3 h at 4°C, washed thrice with 500 εl of 1x TBS-MNGZ (50 mM Tris-HCl pH 7.4, 150 mM NaCl, 2.5 mM $MgCl_2$, 0.1% NP-40, 10% glycerol) and TEV cleavage buffer (10 mM Tris-HCl pH 7.4, 150 mM NaCl, 0.1% NP-40, 0.5 mM EDTA, 1 mM DTT). Tagged proteins were cut off the beads using 200 units of TEV protease (Life Technologies Europe BV) in a 300 εl reaction for 16 h, at 4 °C. TEV protease cleaved protein complexes, were eluted with 500 εl of 1x TBS-MNGZ and collected. The TEV eluates were incubated with 200 εl of packed Streptavidin beads (Sigma-Aldrich Finland Oy), previously washed with 1 ml of 1x TBS-MNGZ, for 4 h at 4 °C. Bound Streptavidin resin was washed thrice with 500 εl of 1x TBS-MNGZ and competitively eluted by 2.5 mM Biotin diluted in TBS-MNGZ, with gentle end-over-end rotation for 30 min at 4 °C.

2.6. Sample preparation and nano-LC/ESI/MS/MS analysis

Streptavidin eluates (purified protein complexes) were reduced in 20 mM ammonium bicarbonate (Sigma) with 10 mM DTT (Sigma), 2 mM TCEP (Life Technologies Europe BV) (45 min. at 56°C) and alkylated with 55 mM iodoacetamide (Sigma; 30 min. at room temperature, in the dark), prior to TCA / Acetone precipitation. Pellets were dried and solubilised in 0.05% RapiGest SF (186002122; Waters AB, Sweden) by incubation at 60 °C for 30 minutes. Samples were digested overnight with sequencing Grade Modified Trypsin (0.25 - 0.5 µg, V5111, Promega AB), at 37 °C with gentle agitation. The peptide mixture was applied to RP-18 precolumn (nanoACQUITY Symmetry® C18, 186003514; Waters AB) using water containing 0.1% TFA as mobile phase and then separated on a nano-HPLC RP-18 column (nanoACQUITY BEH C18, 186003545; Waters AB) with an acetonitrile gradient (0 % - 60 % ACN in 120 min.), in the presence of 0.05% formic acid at a flow rate of 150 nl/min. The column outlet was directly coupled to the ion source of the spectrometer working in the regime of data dependent MS to MS/MS switch. A blank run ensuring lack of cross contamination from previous samples preceded each analysis.

2.7. Bioinformatic analyses

For details of bioinformatic analyses please see Supplementary material. The networks were drawn using Cytoscape software (http://www.cytoscape.org/) [54].

3. RESULTS

3.1. Establishment of SH-SY5Y stable cells and processing of protein complexes

In order to determine CLN3 IP, we opted for an unbiased five step approach as follows: construction of mammalian retroviral based expression vectors, generation of stably

expressing cell lines, Tandem Affinity Purification (TAP), shot-gun sequencing of isolated protein complexes and functional annotation / interactome analysis (Figure 1).

[Suggested location for Figure 1]

The pCeMM-NTAP(GS)-Gw vector (EUROSCARF; http://web.uni-frankfurt.de/fb15/mikro/euroscarf/index.html) used in this study has previously been described by Bürckstümmer et al. [48]. It has retroviral packaging, a property that was exploited to infect SH-SY5Y cells and also contains a Green fluorescent protein (GFP) cassette which allows for selection of GFP positive cells by flow cytometry. We determined partial sub-cellular localisation of the CLN3 protein in lysosomes and confirmed successful generation of SH-SY5Y-NTAP-CLN3 stable cells, by immunofluorescence confocal microscopy (Figure 2A) and Western blot analysis (Figure 2B). Empty SH-SY5Y cells and SH-SY5Y-NTAP (empty vector) cells served as negative controls.

Two bands (at approx. 60 and smear at 75 kDa; Figure 2B, right), visible on the SH-SY5Y-NTAP-CLN3 lane and absent in the negative controls (SH-SY5Y and SH-SY5Y-NTAP cells) were attributed to glycosylated full-length, tagged CLN3 protein (isoform 1, 438 aminoacids), predicted to migrate about 75 kDa and its un-glycosylated form (at approx. 60 kDa), respectively. It is known that CLN3 is heavily N-glycosylated [55, 56] and typically proteins with this modification tend to migrate at a higher molecular weight than their theoretical values. Endogenously expressed CLN3 in SH-SY5Y cells is undetectable by available CLN3 antibodies and as such no signal of CLN3 was observed in negative controls.

[Suggested location for Figure 2]

Additionally, the vector consists of an N-terminal TAP tag: 2 Protein G, Tobacco etch virus (TEV) site and Streptavidin binding peptide (SBP) domains, which facilitate tandem affinity purification [48]. This feature was utilised to isolate protein complexes from the SH-SY5Y stable cells by Tandem Affinity Purification (TAP; various procedure steps are shown in Supplementary Figure 1A-B), prior to analysis using reverse phase nano-flow Liquid chromatography Electrospray Ionisation coupled to tandem mass spectrometry (reverse phase nano-LC/ESI/MS/MS).

3.2. Identification of Novel CLN3 IP

Protein identifications of CLN3 IP (Table 1) are derived from three independent TAP-MS experiments, in which native protein complexes were isolated from SH-SY5Y-NTAP-CLN3 stable cell lines. SH-SY5Y-NTAP (empty vector) served as the negative control. Bait recovery of tandem affinity purified SH-SY5Y-NTAP-CLN3 (Supplementary Figure 1A) indicates an average of 8 peptides with 26% coverage, for the CLN3 protein (Supplementary Figure 1B). All negative control samples (NTAP) showed no evidence of CLN3 detectable by mass spectrometry (MS). Fragment ion spectra from two representative peptides detectable in the NTAP-CLN3 purified protein complex are depicted in Supplementary Figure 1C. Identifications were accepted for proteins appearing in at least two experiments with an average of individual probabilities for SAINT analysis (AvgP SAINT) Ó 0.50, after exclusion of contaminants (proteins that bind non-specifically to empty vector alone and previously observed TAP contaminants) [48, 57]. Additionally, single protein hits were considered positively identified at a higher threshold of AvgP SAINT Ó 0.90. 35 proteins were in the first category, and 23 in the latter. In total, 58 CLN3 IP were identified in this study, including 42 novel CLN3 IP and 16 CLN3 high confidence interacting partners (HCIP) previously determined by

Behrends et al. 2010 [8]. The unfiltered list of proteins isolated from SH-SY5Y-NTAP-CLN3 stable cells is shown in Supplementary Table 1.

[Suggested location for Table. 1]

3.3. Validation of selected CLN3 IP by co-immunoprecipitation and immunofluorescence co-localisation with CLN3

In order to determine physical interactions of CLN3 with selected IP, we chose 6 CLN3 IP identified by MS (including four of the previously identified CLN3 HCIP in HEK 293 cells [8]) on the basis of their known biological functions or entry clone availability and performed co-immunoprecipitation experiments in HEK 293 cells (Figure 3). This model was chosen since SH-SY5Y cells are slow growing, and thus not very well suited for medium throughput co-immunoprecipitation experiments as opposed to fast growing HEK 293 cells. Moreover, several high-throughput PPI network studies utilised HEK 293 cells in large scale co-immunoprecipitation validation experiments in the past, e.g. [8, 10, 58]. HEK 293 also served as a model in a recent article on autophagy [8], where several partners of CLN3 were detected. The chosen proteins included: two novel CLN3 IP, dopamine beta hydroxylase (DBH), selected for its involvement in the neurological disorders (Supplementary Tables 2 and 3) and dolichol-phosphate mannosyltransferase (DPM1), selected for its role in N-glycosylation and O-mannosylation of proteins.

[Suggested location for Figure 3]

In summary, co-immunoprecipitation analysis (Figure 3) confirmed CLN3 physical interactions with DBH, DPM1, SEC61A1 and SLC25A10. We were unable to detect specific interactions of CLN3 with SLC25A11 and SLC25A22 (data not shown), which suggests that

these interactions may require more specific conditions that were absent in our experimental setup. Alternatively, tagging might have interfered with the interaction. Probing with mouse monoclonal anti-V5 and rabbit polyclonal anti-PA antibodies confirmed approx. 70% of the selected CLN3 IP observed in TAP-MS experiments, including 2 that are common IP to both CLN3 and CLN5 baits.

We further performed *in vivo* subcellular co-localisation studies in SH-SY5Y cells to examine the spatial overlap between DBH, DPM1, SEC61A1, SLC25A10 and CLN3. SH-SY5Y-NTAP-CLN3 stable cells were transiently transfected with the CLN3 IP and analysed for co-localisation patterns by dual immunofluorescence confocal microscopy. This work showed CLN3 to partially co-localise with DBH, DPM1, SEC61A1 and SLC25A10 (Supplementary Figure 2). The distribution of co-localisation points suggests that the interactions between CLN3 and DBH or DPM1 likely occur in lysosomes, whereas those with SEC61A1 and SLC25A10 are in the ER-Golgi and ER, respectively.

3.4. Functional annotation of the CLN3 interactome revealed enrichment in transmembrane transport, generation of precursor metabolites and energy, lipid biosynthesis and nitrogen compound biosynthetic process

Following the identification of CLN3 IP, there was a need to functionally annotate the obtained protein list and analyse the resulting CLN3 interactome. Towards this goal, we initiated GO analysis of the CLN3 interactome by DAVID [47], a publicly available online resource for comprehensive analysis and attachment of biological relevance to gene / protein datasets. Using the human genome as a background, this analysis yielded the following four most enriched GO_biological process terms: transmembrane transport (GO:0055085, fold enrichment: 7.0); generation of precursor metabolites and energy (GO:0006091, fold

enrichment: 5.9); lipid biosynthesis process (GO:0008610, fold enrichment: 5.7) and nitrogen compound biosynthetic process (GO:0044271, fold enrichment: 5.7; Figure 4A and Supplementary Table 4A). The fold enrichment of a particular GO term refers to the ratio of input genes / proteins associated with a specific process or function to the ratio of background information related to the same genes / proteins. For instance 7% of input proteins are associated with transmembrane transport and the background information of proteins associated with the same term is 1%, hence the fold enrichment of 7. Previous studies have implicated CLN3 in transmembrane transport [31, 32, 34], lipid biosynthesis [38], and nitrogen compound biosynthetic process [59], which are also supported by our findings.

Functional clustering analysis of selected terms from GO categories, protein domains, multiple cellular pathways, SwissProt database terms and others (Supplementary Tables 4A-D) revealed that transmembrane transport was the most prominent GO_biological process term in the second most enriched cluster (enrichment score = 7.69, Figure 4B and Supplementary Table 4B). Moreover, cluster 4 (enrichment score = 3.47, Figure 4C and Supplementary Table 4B) included proteins enriched in Huntington's and Parkinson's diseases (KEGG pathway). Functional annotation cluster analysis relies on kappa statistics and fuzzy heuristic clustering, to quantitatively measure the degree of the common genes between two annotations terms. Genes that share a similar set of annotation terms will have a higher chance of being grouped together and likely be involved in similar biological mechanisms [47].

[Suggested location for Figure 4]

3.5. Analysis of the CLN5 interactome

The same experimental procedures used for analysis of the CLN3 interactome, such as generation of stable cell lines and TAP-MS were applied to CLN5. However, pES-CTAP-Puro (a modified version of pCeMM-CTAP(SG)-Gw vector, EUROSCARF), hereby referred to as (CTAP-Puro) was used instead. It is similar to the original plasmid [48], except that the IRES-GFP cassette has been replaced with IRES-Puro and thereby facilitating selection on puromycin (data not shown). The functionality of pES-CTAP-Puro was verified by successful cloning and expression of human CLN5 (Supplementary Figure 3). In this study, no NCL proteins were observed to co-purify with either the CLN3 or CLN5 baits. However, the identified 31 CLN5 IP included 18 proteins in common with the NTAP-CLN3 bait (Figure 5A), 11% of which were verified by co-immunoprecipitation experiments. The common proteins to both CLN3 and CLN5 baits were: SLC25A4, DBH, SFXN3, RCN2, CALU, SLC25A13, SLC25A22, SLC25A1, ATP2A2, SLC25A5, SLC25A6, PHGDH, ARF4, SEC61A1, XPO1, RPN1, SLC25A11 and CDS2. A list of the CLN5 IP, isolated from SH-SY5Y-CLN5-CTAP-Puro stable cells, is shown in Table 2 and the complete unfiltered list of proteins recovered from the cells is presented in Supplementary Table 5.

[Suggested location for Table 2]

3.6. Neurodegenerative disease proteins within the CLN3-CLN5 interactome are linked to mental retardation and epileptic seizures

By linking the combined CLN3-CLN5 interactome to OMIM database we found that 8 of the IP can be assigned to a disease (Supplementary Tables 2 and 3), with 6 of them to a neurodegenerative phenotype. The CLN3-CLN5 interactome (Figure 5A) includes in total 8 neurodegenerative disease causative proteins: CLN3- Batten disease, STRA6- mental

retardation, TECR- nonsyndromic mental retardation, DBH- schizophrenia, PHGDH- psychomotor retardation and seizures, SLC25A22- neonatal myoclonic epilepsy, CLN5- Finnish variant late infantile NCL and ATP1A3- dystonia parkinsonism. Most of these proteins are either involved in mental retardation or epileptic seizures, both of which are established clinical symptoms of NCL patients. Interestingly, 4 CLN3 IP can be further assigned to Huntington's disease (KEGG pathway; hsa: 05016) and Parkinson's disease (hsa: 05012) pathways (SLC25A6, SLC25A5, SLC25A4 and UQCRC2; Figure 4C, Supplementary Figure 4 and Supplementary Tables 4B and 4D). Moreover, a functional linkage between those proteins and synuclein can be established (Supplementary Figure 5). It has recently been demonstrated that CLN3 binds directly to synuclein (SNCA) [60] and several IP from the CLN3-CLN5 network are directly interacting with it (Supplementary Figure 5 and Supplementary Table 6). Other proteins of interest within the network include: ARF3, ARF4 and ARF5, which are GTP-ases of the RAS superfamily that have roles in vesicular trafficking and recruitment of coat complexes to budding vesicles. ARF3 was recently shown to be a constituent of the amyloid η precursor protein (AηPP) interactome in the brain of transgenic mice expressing tagged AηPP [58]. Moreover, FKBP8 and CANX are noteworthy for their anti-apoptotic effects / interactions with PSEN1 / PSEN2 and involvement in dysmyelination, respectively [61, 62]. A more detailed CLN3-CLN5 interactome network that incorporates IP from this work and also includes those derived from other studies (based on literature mining and database knowledge) is depicted in Supplementary Figure 5, for completeness of the available knowledge. A total of 128 proteins including six NCL disease ones (PPT1, TPP1, CLN3, CLN5, CLN6, CLN8) are connected via 162 PPI.

[Suggested location for Figure 5]

4. DISCUSSION

Highly hydrophobic integral membrane proteins like CLN3 present a considerable challenge for interactomics studies, because they are difficult to solubilise and prone to non-specific interactions. In this study, we employed a stringent TAP-MS strategy complemented by bioinformatics, SAINT analysis and co-immunoprecipitation assays, in an attempt to remedy these limitations and draft the CLN3 interactome in SH-SY5Y human neuroblastoma cells. We supplemented our lysis buffer with 1% Nonidet P-40, a nonionic non-denaturing detergent that is sufficient to solubilise membrane proteins without disrupting their molecular environment. Moreover, the SAINT statistical platform allowed us to assign confidence scores to PPI deduced from our TAP-MS experiments. SAINT uses label free quantitative data (spectral counts), to derive a probability of true interaction and is an efficient tool to discern true interaction partners from background noise, even in instances when the proteins are detected at low levels in control samples [46].

The choice of cellular model was motivated by a need to mimic the physiological context of CLN3 disease, which involves degeneration of cortical neurons. As such, we chose SH-SY5Y human neuroblastoma cells, an established dopaminergic neuron model that has been extensively used for studies of Parkinson's disease [63] and CLN3 function [26, 64, 65]. Moreover, CLN3 patients have Parkinsonian symptoms and decreased dopamine transporter density in the striatum [66]. Therefore, we isolated protein complexes from SH-SY5Y stable cells and based on three independent TAP-MS experiments, a total of 58 CLN3 IP (Table 1) was identified after SAINT analysis and filtration of known contaminants [48, 57]. They included 42 novel CLN3 IP and 16 CLN3 HCIP previously found by Behrends et al. [8], thereby confirming the reliability of our approach. TAP is especially well suited for isolation of TAP-tagged CLN3 protein complexes, because the currently available antibodies do not detect the

endogenously expressed protein. It is noteworthy that PPI derived from a TAP-MS platform may include both direct and indirect interactors. Moreover, our draft CLN3 interactome is likely incomplete, since TAP technology inherently limits the recovery of more transient interactions during the two step affinity purification.

In this study, we confirmed the CLN3 interaction with Na+-K+-ATPase [40] and also successfully reproduced 37% of the 43 CLN3 HCIP determined in a single affinity-capture MS dataset from HEK 293 cells [8]. Other reported interactions were not verified by our TAP-MS approach, for several reasons. Firstly, CLN3 interactions with ß-fodrin [40], calsenilin [26], SBDS [28, 42] and myosin IIB [28], were determined by Y2H screens and the Cytotrap Y2H system, respectively. Secondly, CLN3 interactions with Rab7 [41], RILP [41] and Hook 1 [33], were detected by immunofluorescence confocal microscopy in HeLa cells. This discrepancy is probably explained by the fact that both methodologies are significantly different from our approach which assays protein complexes at close to endogenous levels in human neuroblastoma cells.

In order to explore further the connectivity of both CLN3 and CLN5 interactomes, we systematically surveyed mammalian protein complexes using Corum database (http://mips.gsf.de/genre/proj/corum/index.html), a collection of experimentally verified mammalian protein complexes. For example, SLC25A5, together with SLC25A4 and ATP5A1 form SDH-mABC1-PIC-ANT-ATPase complex (Corum complex:139; Figure 5B), while ATP1A1 together with ATP1B1 are part of Na^+, K^+-ATPase complex (Corum complex:3134; Figure 4B and C; Supplementary Table 2). ATP1B1 has previously been detected as a CLN3 IP in yeast- two hybrid screens [67].

Most notable of the previously identified CLN3 IP are PHGDH and SLC25A22, for their involvement in L-serine synthesis and neuronal excitability, respectively. 3-

phosphoglycerate dehydrogenase (PHGDH) catalyses a critical first step in the biosynthesis of L-serine. The importance of L-serine in cellular metabolism is derived from its essential roles as a precursor for the synthesis of proteins, membrane lipids, and neuromodulators (glycine and D-serine). Patients with PHGDH deficiency (OMIM: 601815) are characterised by congenital microcephaly, psychomotor retardation, and seizures [68, 69]. Mutations in the mitochondrial glutamate carrier SLC25A22 cause neonatal myoclonic epilepsy (OMIM: 609304), whose symptoms include, spontaneous muscle contractions, hypotonia, microcephaly, abnormal optic nerve conduction, rapid evolution into general brain dysfunction and spasticity [70, 71]. Moreover, results from patients' fibroblasts showed that alterations in mitochondrial glutamate import / metabolism led to impaired neuronal excitability [72]. It is postulated that a failure of mitochondrial glutamate transport in astrocytes leads to accumulation of glutamate in the cytosol and thereby neuronal synchronicity that contributes to epileptic seizures [70]. Although, CLN3 associations with PHGDH and SLC25A22 have previously been shown in HEK 293 cells [8], this study provides the first such evidence in a neuronal-like cell line.

Three novel CLN3 IP were of particular interest because of their involvement in G-protein signalling (CDS2 and PTPLAD1) and protein folding / sorting in the ER (CALU). CDP-diacylglycerol synthase (CDS2) encodes an integral membrane protein that catalyses the conversion of phosphatidic acid to CDP-diacylglycerol and is localised in both the inner mitochondrial matrix membrane and cytoplasmic side of the endoplasmic reticulum (ER). The enzyme is involved in the synthesis of phosphatidylglycerol and cardiolipin, in mitochondria and phosphatidylinositol biosynthesis, in the ER [73]. In *Cln3* deficient mouse cerebellar cells where autophagy was impaired [25], inositol monophosphatase inhibitors which affect the phosphatidyl inositol signalling pathway, partially rescued the autophagic process and

reduced the neuronal vulnerability in these cells [74]. Interestingly, recent work in *C. elegans* shows that synaptic polarity depends on phosphatidylinositol signalling regulated by myo-inositol monophosphatase [75], thus potentially providing a mechanistic link between the observations of impaired autophagy, phosphatidylinositol signalling, synaptic failure and apoptosis.

Another protein involved in signalling is Protein-tyrosine phosphatase-like A domain containing 1 protein (PTPLAD1), an integral membrane protein implicated in small GTPase mediated signal transduction and fatty acid biosynthetic process [76, 77]. The third novel CLN3 IP, Calumenin (CALU), is a calcium binding protein that is highly expressed in various brain regions during development and functions in protein folding and sorting in the ER [78]. The surveyed novel CLN3 IP, support functional roles of the protein in GTPase mediated signal transduction and involvement in the ER quality control machinery. Moreover, this study establishes a novel link between CLN3 and the regulation of cellular phospholipid content through its interaction with CDS2.

An indirect interaction between CLN3 and CLN5 proteins was reported in GST-pulldown experiments when overexpressed CLN3 and CLN5 fragments were used [79]. In this study, a molecular link between NCL proteins is supported by the common proteins co-purified with both CLN3 and CLN5 baits (Figure 5A). The majority of these proteins are mitochondrial carriers (SLC25A4, SLC25A13, SLC25A22, SLC25A1, SLC25A5, SLC25A6 and SLC25A11), involved in neurodegenerative diseases (DBH, PHGDH and SLC25A22; Supplementary Table 3) or calcium binding (CALU, RCN2). Moreover, since all NCL are related to deposition of storage material, we systematically searched for known components of lipofuscin. Intriguingly, 10 proteins (14%) of the combined CLN3-CLN5 interactome are constituents of the lipofuscin proteome (Supplementary Table 2) [80, 81].

Most identified CLN3 and CLN5 IP are novel and so in order to gain more insight into their functional associations using network approaches, we utilised FunCoup database (http://FunCoup.sbc.su.se, [82]) which allows for visualisation of global gene / protein networks of functional coupling via Bayesian integration of diverse high-throughput data. Among the 67 out of 72 input genes present in the FunCoup, we identified 649 functionally coupled pairs with high confidence score (Ó 0.5, scale 0-1; Supplementary Table 7). 14 of the 55 (22%) CLN3 IP, including two novel ones (SCAMP3 and TECR) are predicted to be functionally coupled with CLN3 at this threshold. CLN5 is predicted to be functionally linked with CLN3 at a very high confidence level of 0.96 and with SEL1L protein (score = 0.93). The high number of links (approx. 10) per protein reflects a dense network of functional associations among the input genes providing further support for their involvement in similar biological processes.

In an attempt to functionally cluster the CLN3-CLN5 bridging proteins, we also queried their direct IP and filtered for high expression in the brain (http://cbdm.mdc-berlin.de/tools/hippie/information.php, [83]). Several mitochondrial carriers were connected through proteins involved in autophagy (Supplementary Figure 6), a process in which CLN3 has previously been implicated [8, 25]. Moreover, as GABAergic neuronal populations are strongly affected in both CLN3 and CLN5 patients especially in the CA2-CA4 regions of the hippocampus [84], it is plausible that autophagic processes involving GABA-receptor associated proteins may be responsible for neurodegenerative processes in these brain regions.

Previous work by Oresic et al. 2009 [85] demonstrated that CLN6 (also predicted to interact with CLN5; overall probability score = 0.36, medium confidence range; PrePPI database, http://bhapp.c2b2.columbia.edu/PrePPI/ [86, 87]) mutants (G123D and M241T), formed a complex with proteins of the ERAD pathway and could be significantly rescued with knockdown of SEL1L. Interestingly, several proteins of the ERAD pathway (SEL1L, OS9,

FBXO6 and FBX27) co-purified with the CLN5 bait. These findings indicate a functional link between CLN5 and CLN6, at the ER quality control. Although no NCL proteins co-purified with either the CLN3 or CLN5 baits, the common proteins between the two suggest that interactions amongst NCL proteins maybe transient. Given the underlying phenotype similarities of NCL disorders, the assumption of common molecular mechanisms seems plausible.

Conclusions

These findings demonstrate that the TAP-MS approach, combined with bioinformatics, SAINT analysis and co-immunoprecipitation assays is a valid platform for investigating interactomes of low abundance integral membrane proteins. Specifically, this study revealed that the combined CLN3-CLN5 interactome in SH-SY5Y human neuroblastoma cells includes proteins involved in neurodegeneration, mental retardation and epileptic seizures. The extent of crosstalk amongst disease proteins is marked and may suggest that the mechanisms leading to the functional deficits are shared between them. Here, previously suggested functional roles of CLN3 in transmembrane transport, lipid homeostasis and neuronal excitability, are also supported by our data. Furthermore, this study proposes new roles of CLN3 in G-protein signalling and protein folding / sorting in the ER.

Acknowledgments

We thank Dr. Frank Liu (Samuel Lunenfeld Research Institute, University of Toronto, Canada) for assistance with SAINT analysis, Dr. Aija Kyttälä and Dr. Mia-Lisa Schmiedt (Public Health Genomics Unit, Department of Chronic Disease Prevention, National Institute for Health and Welfare, Helsinki, Finland) for discussions on CLN5. MSc. Rabah Soliymani and MSc. Guzel Kireeva (Meilahti Clinical Proteomics Facility, University of Helsinki, Finland) for discussions on sample preparation for mass spectrometry and technical assistance / discussion on the manuscript, respectively. Dr. Lucia Napione (Institute for Cancer Research and Treatment, University of Torino, Italy) is acknowledged for critically reviewing the manuscript. Confocal imaging was done at the Molecular Imaging Unit, Biomedicum Helsinki. This work was supported by the Finnish Academy of Science 128600 grant (to M.L) and also received partial funding from the European Union Seventh Framework Programme (FP7/2007-2013) under grant agreement n° 281234". We finally wish to thank CHEMSEM graduate school for financial support.

Supporting Information Available:

Supplementary Figure 1, Isolation of CLN3 IP by TAP and bait recovery. Supplementary Figure 2, Immunofluorescence co-localisation of CLN3 with selected IP in SH-SY5Y cells. Supplementary Figure 3, Generation of SH-SY5Y-CLN5-CTAP-Puro stable cells. Supplementary Figure 4, Parkinson's disease KEGG pathway involvement. Supplementary Figure 5, Comprehensive Cytoscape map of the CLN3-CLN5 interactome. Supplementary Figure 6, Brain network analysis of CLN3-CLN5 bridging proteins. Supplementary Table 1A-C, Unfiltered list of proteins isolated from SH-SY5Y-NTAP-CLN3 stable cells (Exp.1-3). Supplementary Table 2, List of all CLN3 and CLN5 IP with Gene identifiers, complex attributes and OMIM phenotypes. Supplementary Table 3, List of literature derived disease associations of CLN3-CLN5 network. Supplementary Table 4A, Summary list of GO_Biological Process classification and other functional terms of CLN3 IP identified by TAP-MS. Supplementary Table 4B, Functional cluster term enrichment analysis of CLN3 IP. Supplementary Table 4C, Functional cluster term enrichment analysis of CLN5 IP. Supplementary Table 4D, List of over-represented pathways for CLN3 and CLN5 local networks. Supplementary Table 5A-C, Unfiltered list of proteins isolated from SH-SY5Y-CLN5-CTAP-Puro stable cells (Exp.1-3). Supplementary Table 6, List of all known interactions of combined CLN3-CLN5 network. Supplementary Table 7, Predicted functional links between CLN3-CLN5 network proteins. This Information is available free of charge via the internet at http://pubs.acs.org

REFERENCES

(1) Alberts, B., The cell as a collection of protein machines: preparing the next generation of molecular biologists. *Cell* **1998,** 92, (3), 291-4.
(2) Barrios-Rodiles, M.; Brown, K. R.; Ozdamar, B.; Bose, R.; Liu, Z.; Donovan, R. S.; Shinjo, F.; Liu, Y.; Dembowy, J.; Taylor, I. W.; Luga, V.; Przulj, N.; Robinson, M.; Suzuki, H.; Hayashizaki, Y.; Jurisica, I.; Wrana, J. L., High-throughput mapping of a dynamic signaling network in mammalian cells. *Science* **2005,** 307, (5715), 1621-1625.
(3) Gavin, A. C.; Bosche, M.; Krause, R.; Grandi, P.; Marzioch, M.; Bauer, A.; Schultz, J.; Rick, J. M.; Michon, A. M.; Cruciat, C. M.; Remor, M.; Hofert, C.; Schelder, M.; Brajenovic, M.; Ruffner, H.; Merino, A.; Klein, K.; Hudak, M.; Dickson, D.; Rudi, T.; Gnau, V.; Bauch, A.; Bastuck, S.; Huhse, B.; Leutwein, C.; Heurtier, M. A.; Copley, R. R.; Edelmann, A.; Querfurth, E.; Rybin, V.; Drewes, G.; Raida, M.; Bouwmeester, T.; Bork, P.; Seraphin, B.; Kuster, B.; Neubauer, G.; Superti-Furga, G., Functional organization of the yeast proteome by systematic analysis of protein complexes. *Nature* **2002,** 415, (6868), 141-7.
(4) Gingras, A. C.; Aebersold, R.; Raught, B., Advances in protein complex analysis using mass spectrometry. *J Physiol* **2005,** 563, (Pt 1), 11-21.
(5) Rual, J. F.; Venkatesan, K.; Hao, T.; Hirozane-Kishikawa, T.; Dricot, A.; Li, N.; Berriz, G. F.; Gibbons, F. D.; Dreze, M.; Ayivi-Guedehoussou, N.; Klitgord, N.; Simon, C.; Boxem, M.; Milstein, S.; Rosenberg, J.; Goldberg, D. S.; Zhang, L. V.; Wong, S. L.; Franklin, G.; Li, S.; Albala, J. S.; Lim, J.; Fraughton, C.; Llamosas, E.; Cevik, S.; Bex, C.; Lamesch, P.; Sikorski, R. S.; Vandenhaute, J.; Zoghbi, H. Y.; Smolyar, A.; Bosak, S.; Sequerra, R.; Doucette-Stamm, L.; Cusick, M. E.; Hill, D. E.; Roth, F. P.; Vidal, M., Towards a proteome-scale map of the human protein-protein interaction network. *Nature* **2005,** 437, (7062), 1173-1178.
(6) Stelzl, U.; Worm, U.; Lalowski, M.; Haenig, C.; Brembeck, F. H.; Goehler, H.; Stroedicke, M.; Zenkner, M.; Schoenherr, A.; Koeppen, S.; Timm, J.; Mintzlaff, S.; Abraham, C.; Bock, N.; Kietzmann, S.; Goedde, A.; Toksoz, E.; Droege, A.; Krobitsch, S.; Korn, B.; Birchmeier, W.; Lehrach, H.; Wanker, E. E., A human protein-protein interaction network: a resource for annotating the proteome. *Cell* **2005,** 122, (6), 957-968.
(7) Venkatesan, K.; Rual, J. F.; Vazquez, A.; Stelzl, U.; Lemmens, I.; Hirozane-Kishikawa, T.; Hao, T.; Zenkner, M.; Xin, X.; Goh, K. I.; Yildirim, M. A.; Simonis, N.; Heinzmann, K.; Gebreab, F.; Sahalie, J. M.; Cevik, S.; Simon, C.; de Smet, A. S.; Dann, E.; Smolyar, A.; Vinayagam, A.; Yu, H.; Szeto, D.; Borick, H.; Dricot, A.; Klitgord, N.; Murray, R. R.; Lin, C.; Lalowski, M.; Timm, J.; Rau, K.; Boone, C.; Braun, P.; Cusick, M. E.; Roth, F. P.; Hill, D. E.; Tavernier, J.; Wanker, E. E.; Barabasi, A. L.; Vidal, M., An empirical framework for binary interactome mapping. *Nat. Methods* **2009,** 6, (1), 83-90.
(8) Behrends, C.; Sowa, M. E.; Gygi, S. P.; Harper, J. W., Network organization of the human autophagy system. *Nature* **2010,** 466, (7302), 68-76.
(9) Ewing, R. M.; Chu, P.; Elisma, F.; Li, H.; Taylor, P.; Climie, S.; McBroom-Cerajewski, L.; Robinson, M. D.; O'Connor, L.; Li, M.; Taylor, R.; Dharsee, M.; Ho, Y.; Heilbut, A.; Moore, L.; Zhang, S.; Ornatsky, O.; Bukhman, Y. V.; Ethier, M.; Sheng, Y.; Vasilescu, J.; Abu-Farha, M.; Lambert, J. P.; Duewel, H. S.; Stewart, II; Kuehl, B.; Hogue, K.; Colwill, K.; Gladwish, K.; Muskat, B.; Kinach, R.; Adams, S. L.; Moran, M. F.; Morin, G. B.; Topaloglou, T.; Figeys, D., Large-scale mapping of human protein-protein interactions by mass spectrometry. *Mol. Syst. Biol.* **2007,** 3, 89.

(10) Sowa, M. E.; Bennett, E. J.; Gygi, S. P.; Harper, J. W., Defining the human deubiquitinating enzyme interaction landscape. *Cell* **2009,** 138, (2), 389-403.
(11) Li, S.; Armstrong, C. M.; Bertin, N.; Ge, H.; Milstein, S.; Boxem, M.; Vidalain, P. O.; Han, J. D.; Chesneau, A.; Hao, T.; Goldberg, D. S.; Li, N.; Martinez, M.; Rual, J. F.; Lamesch, P.; Xu, L.; Tewari, M.; Wong, S. L.; Zhang, L. V.; Berriz, G. F.; Jacotot, L.; Vaglio, P.; Reboul, J.; Hirozane-Kishikawa, T.; Li, Q.; Gabel, H. W.; Elewa, A.; Baumgartner, B.; Rose, D. J.; Yu, H.; Bosak, S.; Sequerra, R.; Fraser, A.; Mango, S. E.; Saxton, W. M.; Strome, S.; Van Den Heuvel, S.; Piano, F.; Vandenhaute, J.; Sardet, C.; Gerstein, M.; Doucette-Stamm, L.; Gunsalus, K. C.; Harper, J. W.; Cusick, M. E.; Roth, F. P.; Hill, D. E.; Vidal, M., A map of the interactome network of the metazoan *C. elegans*. *Science* **2004,** 303, (5657), 540-543.
(12) Polanowska, J.; Martin, J. S.; Fisher, R.; Scopa, T.; Rae, I.; Boulton, S. J., Tandem immunoaffinity purification of protein complexes from Caenorhabditis elegans. *Biotechniques* **2004,** 36, (5), 778-80, 782.
(13) Giot, L.; Bader, J. S.; Brouwer, C.; Chaudhuri, A.; Kuang, B.; Li, Y.; Hao, Y. L.; Ooi, C. E.; Godwin, B.; Vitols, E.; Vijayadamodar, G.; Pochart, P.; Machineni, H.; Welsh, M.; Kong, Y.; Zerhusen, B.; Malcolm, R.; Varrone, Z.; Collis, A.; Minto, M.; Burgess, S.; McDaniel, L.; Stimpson, E.; Spriggs, F.; Williams, J.; Neurath, K.; Ioime, N.; Agee, M.; Voss, E.; Furtak, K.; Renzulli, R.; Aanensen, N.; Carrolla, S.; Bickelhaupt, E.; Lazovatsky, Y.; DaSilva, A.; Zhong, J.; Stanyon, C. A.; Finley, R. L., Jr.; White, K. P.; Braverman, M.; Jarvie, T.; Gold, S.; Leach, M.; Knight, J.; Shimkets, R. A.; McKenna, M. P.; Chant, J.; Rothberg, J. M., A protein interaction map of Drosophila melanogaster. *Science* **2003,** 302, (5651), 1727-1736.
(14) Guruharsha, K. G.; Rual, J. F.; Zhai, B.; Mintseris, J.; Vaidya, P.; Vaidya, N.; Beekman, C.; Wong, C.; Rhee, D. Y.; Cenaj, O.; McKillip, E.; Shah, S.; Stapleton, M.; Wan, K. H.; Yu, C.; Parsa, B.; Carlson, J. W.; Chen, X.; Kapadia, B.; VijayRaghavan, K.; Gygi, S. P.; Celniker, S. E.; Obar, R. A.; Artavanis-Tsakonas, S., A protein complex network of Drosophila melanogaster. *Cell* **2011,** 147, (3), 690-703.
(15) Ito, T.; Chiba, T.; Ozawa, R.; Yoshida, M.; Hattori, M.; Sakaki, Y., A comprehensive two-hybrid analysis to explore the yeast protein interactome. *Proc. Natl. Acad. Sci. USA* **2001,** 98, (8), 4569-4574.
(16) Figeys, D., Mapping the human protein interactome. *Cell Res.* **2008,** 18, (7), 716-724.
(17) Gingras, A. C.; Gstaiger, M.; Raught, B.; Aebersold, R., Analysis of protein complexes using mass spectrometry. *Nat Rev Mol Cell Biol* **2007,** 8, (8), 645-54.
(18) Berggard, T.; Linse, S.; James, P., Methods for the detection and analysis of protein-protein interactions. *Proteomics* **2007,** 7, (16), 2833-42.
(19) Kaltenbach, L. S.; Romero, E.; Becklin, R. R.; Chettier, R.; Bell, R.; Phansalkar, A.; Strand, A.; Torcassi, C.; Savage, J.; Hurlburt, A.; Cha, G. H.; Ukani, L.; Chepanoske, C. L.; Zhen, Y.; Sahasrabudhe, S.; Olson, J.; Kurschner, C.; Ellerby, L. M.; Peltier, J. M.; Botas, J.; Hughes, R. E., Huntingtin interacting proteins are genetic modifiers of neurodegeneration. *PLoS Genet.* **2007,** 3, (5), e82.
(20) Zhao, R.; Davey, M.; Hsu, Y. C.; Kaplanek, P.; Tong, A.; Parsons, A. B.; Krogan, N.; Cagney, G.; Mai, D.; Greenblatt, J.; Boone, C.; Emili, A.; Houry, W. A., Navigating the chaperone network: an integrative map of physical and genetic interactions mediated by the hsp90 chaperone. *Cell* **2005,** 120, (5), 715-27.
(21) Haltia, M., The neuronal ceroid-lipofuscinoses: from past to present. *Biochim Biophys Acta* **2006,** 1762, (10), 850-6.

(22) Uvebrant, P.; Hagberg, B., Neuronal ceroid lipofuscinoses in Scandinavia. Epidemiology and clinical pictures. *Neuropediatrics* **1997,** 28, (1), 6-8.
(23) Consortium, B. D., Isolation of a novel gene underlying Batten disease, CLN3. The International Batten Disease Consortium. *Cell* **1995,** 82, (6), 949-57.
(24) Luiro, K.; Kopra, O.; Lehtovirta, M.; Jalanko, A., CLN3 protein is targeted to neuronal synapses but excluded from synaptic vesicles: new clues to Batten disease. *Hum Mol Genet* **2001,** 10, (19), 2123-31.
(25) Cao, Y.; Espinola, J. A.; Fossale, E.; Massey, A. C.; Cuervo, A. M.; MacDonald, M. E.; Cotman, S. L., Autophagy is disrupted in a knock-in mouse model of juvenile neuronal ceroid lipofuscinosis. *J Biol Chem* **2006,** 281, (29), 20483-93.
(26) Chang, J. W.; Choi, H.; Kim, H. J.; Jo, D. G.; Jeon, Y. J.; Noh, J. Y.; Park, W. J.; Jung, Y. K., Neuronal vulnerability of CLN3 deletion to calcium-induced cytotoxicity is mediated by calsenilin. *Hum Mol Genet* **2007,** 16, (3), 317-26.
(27) Codlin, S.; Mole, S. E., S. pombe btn1, the orthologue of the Batten disease gene CLN3, is required for vacuole protein sorting of Cpy1p and Golgi exit of Vps10p. *J Cell Sci* **2009,** 122, (Pt 8), 1163-73.
(28) Getty, A. L.; Benedict, J. W.; Pearce, D. A., A novel interaction of CLN3 with nonmuscle myosin-IIB and defects in cell motility of Cln3(-/-) cells. *Exp Cell Res* **2011,** 317, (1), 51-69.
(29) Golabek, A. A.; Kida, E.; Walus, M.; Kaczmarski, W.; Michalewski, M.; Wisniewski, K. E., CLN3 protein regulates lysosomal pH and alters intracellular processing of Alzheimer's amyloid-beta protein precursor and cathepsin D in human cells. *Mol Genet Metab* **2000,** 70, (3), 203-13.
(30) Hobert, J. A.; Dawson, G., A novel role of the Batten disease gene CLN3: association with BMP synthesis. *Biochem Biophys Res Commun* **2007,** 358, (1), 111-6.
(31) Kama, R.; Kanneganti, V.; Ungermann, C.; Gerst, J. E., The yeast Batten disease orthologue Btn1 controls endosome-Golgi retrograde transport via SNARE assembly. *J Cell Biol* **2011,** 195, (2), 203-15.
(32) Kim, Y.; Ramirez-Montealegre, D.; Pearce, D. A., A role in vacuolar arginine transport for yeast Btn1p and for human CLN3, the protein defective in Batten disease. *Proc Natl Acad Sci U S A* **2003,** 100, (26), 15458-62.
(33) Luiro, K.; Yliannala, K.; Ahtiainen, L.; Maunu, H.; Jarvela, I.; Kyttala, A.; Jalanko, A., Interconnections of CLN3, Hook1 and Rab proteins link Batten disease to defects in the endocytic pathway. *Hum. Mol. Genet.* **2004,** 13, (23), 3017-3027.
(34) Metcalf, D. J.; Calvi, A. A.; Seaman, M.; Mitchison, H. M.; Cutler, D. F., Loss of the Batten disease gene CLN3 prevents exit from the TGN of the mannose 6-phosphate receptor. *Traffic* **2008,** 9, (11), 1905-14.
(35) Narayan, S. B.; Rakheja, D.; Tan, L.; Pastor, J. V.; Bennett, M. J., CLN3P, the Batten's disease protein, is a novel palmitoyl-protein Delta-9 desaturase. *Ann Neurol* **2006,** 60, (5), 570-7.
(36) Padilla-Lopez, S.; Pearce, D. A., Saccharomyces cerevisiae lacking Btn1p modulate vacuolar ATPase activity to regulate pH imbalance in the vacuole. *J Biol Chem* **2006,** 281, (15), 10273-80.
(37) Ramirez-Montealegre, D.; Pearce, D. A., Defective lysosomal arginine transport in juvenile Batten disease. *Hum Mol Genet* **2005,** 14, (23), 3759-73.

(38) Rusyn, E.; Mousallem, T.; Persaud-Sawin, D. A.; Miller, S.; Boustany, R. M., CLN3p impacts galactosylceramide transport, raft morphology, and lipid content. *Pediatr Res* **2008,** 63, (6), 625-31.
(39) Tuxworth, R. I.; Vivancos, V.; O'Hare, M. B.; Tear, G., Interactions between the juvenile Batten disease gene, CLN3, and the Notch and JNK signalling pathways. *Hum. Mol. Genet.* **2009,** 18, (4), 667-678.
(40) Uusi-Rauva, K.; Luiro, K.; Tanhuanpaa, K.; Kopra, O.; Martin-Vasallo, P.; Kyttala, A.; Jalanko, A., Novel interactions of CLN3 protein link Batten disease to dysregulation of fodrin-Na+, K+ ATPase complex. *Exp Cell Res* **2008,** 314, (15), 2895-905.
(41) Uusi-Rauva, K.; Kyttala, A.; van der Kant, R.; Vesa, J.; Tanhuanpaa, K.; Neefjes, J.; Olkkonen, V. M.; Jalanko, A., Neuronal ceroid lipofuscinosis protein CLN3 interacts with motor proteins and modifies location of late endosomal compartments. *Cell Mol Life Sci* **2012,** 69, (12), 2075-89.
(42) Vitiello, S. P.; Benedict, J. W.; Padilla-Lopez, S.; Pearce, D. A., Interaction between Sdo1p and Btn1p in the Saccharomyces cerevisiae model for Batten disease. *Hum Mol Genet* **2010,** 19, (5), 931-42.
(43) Lane, S. C.; Jolly, R. D.; Schmechel, D. E.; Alroy, J.; Boustany, R. M., Apoptosis as the mechanism of neurodegeneration in Batten's disease. *J Neurochem* **1996,** 67, (2), 677-83.
(44) Borroto-Escuela, D. O.; Correia, P. A.; Romero-Fernandez, W.; Narvaez, M.; Fuxe, K.; Ciruela, F.; Garriga, P., Muscarinic receptor family interacting proteins: role in receptor function. *J Neurosci Methods* **2011,** 195, (2), 161-9.
(45) Schalm, S. S.; Ballif, B. A.; Buchanan, S. M.; Phillips, G. R.; Maniatis, T., Phosphorylation of protocadherin proteins by the receptor tyrosine kinase Ret. *Proc Natl Acad Sci U S A* **2010,** 107, (31), 13894-9.
(46) Skarra, D. V.; Goudreault, M.; Choi, H.; Mullin, M.; Nesvizhskii, A. I.; Gingras, A. C.; Honkanen, R. E., Label-free quantitative proteomics and SAINT analysis enable interactome mapping for the human Ser/Thr protein phosphatase 5. *Proteomics* **2011,** 11, (8), 1508-16.
(47) Huang da, W.; Sherman, B. T.; Lempicki, R. A., Systematic and integrative analysis of large gene lists using DAVID bioinformatics resources. *Nat. Protoc.* **2009,** 4, (1), 44-57.
(48) Burckstummer, T.; Bennett, K. L.; Preradovic, A.; Schutze, G.; Hantschel, O.; Superti-Furga, G.; Bauch, A., An efficient tandem affinity purification procedure for interaction proteomics in mammalian cells. *Nat. Methods* **2006,** 3, (12), 1013-1019.
(49) DuBridge, R. B.; Tang, P.; Hsia, H. C.; Leong, P. M.; Miller, J. H.; Calos, M. P., Analysis of mutation in human cells by using an Epstein-Barr virus shuttle system. *Mol Cell Biol* **1987,** 7, (1), 379-87.
(50) Pear, W. S.; Nolan, G. P.; Scott, M. L.; Baltimore, D., Production of high-titer helper-free retroviruses by transient transfection. *Proc Natl Acad Sci U S A* **1993,** 90, (18), 8392-6.
(51) Sharma, S.; Murai, F.; Miyanohara, A.; Friedmann, T., Noninfectious virus-like particles produced by Moloney murine leukemia virus-based retrovirus packaging cells deficient in viral envelope become infectious in the presence of lipofection reagents. *Proc Natl Acad Sci U S A* **1997,** 94, (20), 10803-8.

(52) Naldini, L.; Blomer, U.; Gallay, P.; Ory, D.; Mulligan, R.; Gage, F. H.; Verma, I. M.; Trono, D., In vivo gene delivery and stable transduction of nondividing cells by a lentiviral vector. *Science* **1996,** 272, (5259), 263-7.
(53) Schmiedt, M. L.; Bessa, C.; Heine, C.; Ribeiro, M. G.; Jalanko, A.; Kyttala, A., The neuronal ceroid lipofuscinosis protein CLN5: new insights into cellular maturation, transport, and consequences of mutations. *Hum Mutat* **2010,** 31, (3), 356-65.
(54) Shannon, P.; Markiel, A.; Ozier, O.; Baliga, N. S.; Wang, J. T.; Ramage, D.; Amin, N.; Schwikowski, B.; Ideker, T., Cytoscape: a software environment for integrated models of biomolecular interaction networks. *Genome Res* **2003,** 13, (11), 2498-504.
(55) Ezaki, J.; Takeda-Ezaki, M.; Koike, M.; Ohsawa, Y.; Taka, H.; Mineki, R.; Murayama, K.; Uchiyama, Y.; Ueno, T.; Kominami, E., Characterization of Cln3p, the gene product responsible for juvenile neuronal ceroid lipofuscinosis, as a lysosomal integral membrane glycoprotein. *J Neurochem* **2003,** 87, (5), 1296-308.
(56) Golabek, A. A.; Kaczmarski, W.; Kida, E.; Kaczmarski, A.; Michalewski, M. P.; Wisniewski, K. E., Expression studies of CLN3 protein (battenin) in fusion with the green fluorescent protein in mammalian cells in vitro. *Mol Genet Metab* **1999,** 66, (4), 277-82.
(57) Vandamme, J.; Volkel, P.; Rosnoblet, C.; Le Faou, P.; Angrand, P. O., Interaction proteomics analysis of polycomb proteins defines distinct PRC1 complexes in mammalian cells. *Mol Cell Proteomics* **2011,** 10, (4), M110 002642.
(58) Kohli, B. M.; Pflieger, D.; Mueller, L. N.; Carbonetti, G.; Aebersold, R.; Nitsch, R. M.; Konietzko, U., Interactome of the amyloid precursor protein APP in brain reveals a protein network involved in synaptic vesicle turnover and a close association with Synaptotagmin-1. *J Proteome Res* **2012,** 11, (8), 4075-90.
(59) Osorio, N. S.; Carvalho, A.; Almeida, A. J.; Padilla-Lopez, S.; Leao, C.; Laranjinha, J.; Ludovico, P.; Pearce, D. A.; Rodrigues, F., Nitric oxide signaling is disrupted in the yeast model for Batten disease. *Mol Biol Cell* **2007,** 18, (7), 2755-67.
(60) Koenn, M. Creating a Protein-Protein Interaction Network for Alpha-Synuclein. PhD Thesis, Free University of Berlin, Berlin, **2012**, 192.
(61) Kraus, A.; Groenendyk, J.; Bedard, K.; Baldwin, T. A.; Krause, K. H.; Dubois-Dauphin, M.; Dyck, J.; Rosenbaum, E. E.; Korngut, L.; Colley, N. J.; Gosgnach, S.; Zochodne, D.; Todd, K.; Agellon, L. B.; Michalak, M., Calnexin deficiency leads to dysmyelination. *J Biol Chem* **2010,** 285, (24), 18928-38.
(62) Wang, H. Q.; Nakaya, Y.; Du, Z.; Yamane, T.; Shirane, M.; Kudo, T.; Takeda, M.; Takebayashi, K.; Noda, Y.; Nakayama, K. I.; Nishimura, M., Interaction of presenilins with FKBP38 promotes apoptosis by reducing mitochondrial Bcl-2. *Hum Mol Genet* **2005,** 14, (13), 1889-902.
(63) Kitao, Y.; Matsuyama, T.; Takano, K.; Tabata, Y.; Yoshimoto, T.; Momoi, T.; Yamatodani, A.; Ogawa, S.; Hori, O., Does ORP150/HSP12A protect dopaminergic neurons against MPTP/MPP(+)-induced neurotoxicity? *Antioxid Redox Signal* **2007,** 9, (5), 589-95.
(64) An Haack, K.; Narayan, S. B.; Li, H.; Warnock, A.; Tan, L.; Bennett, M. J., Screening for calcium channel modulators in CLN3 siRNA knock down SH-SY5Y neuroblastoma cells reveals a significant decrease of intracellular calcium levels by selected L-type calcium channel blockers. *Biochim Biophys Acta* **2011,** 1810, (2), 186-91.
(65) Narayan, S. B.; Rakheja, D.; Pastor, J. V.; Rosenblatt, K.; Greene, S. R.; Yang, J.; Wolf, B. A.; Bennett, M. J., Over-expression of CLN3P, the Batten disease protein, inhibits PANDER-induced apoptosis in neuroblastoma cells: further evidence that CLN3P has anti-apoptotic properties. *Mol Genet Metab* **2006,** 88, (2), 178-83.

(66) Aberg, L. E.; Rinne, J. O.; Rajantie, I.; Santavuori, P., A favorable response to antiparkinsonian treatment in juvenile neuronal ceroid lipofuscinosis. *Neurology* **2001,** 56, (9), 1236-9.
(67) Uusi-Rauva, K., Molecular interactions of Neuronal Ceroid Lipofuscinosis protein CLN3. PhD Thesis, University of Helsinki and National Institute for Health and Welfare (THL) **2012**, 73.
(68) Jaeken, J.; Detheux, M.; Van Maldergem, L.; Foulon, M.; Carchon, H.; Van Schaftingen, E., 3-Phosphoglycerate dehydrogenase deficiency: an inborn error of serine biosynthesis. *Arch Dis Child* **1996,** 74, (6), 542-5.
(69) Klomp, L. W.; de Koning, T. J.; Malingre, H. E.; van Beurden, E. A.; Brink, M.; Opdam, F. L.; Duran, M.; Jaeken, J.; Pineda, M.; Van Maldergem, L.; Poll-The, B. T.; van den Berg, I. E.; Berger, R., Molecular characterization of 3-phosphoglycerate dehydrogenase deficiency--a neurometabolic disorder associated with reduced L-serine biosynthesis. *Am J Hum Genet* **2000,** 67, (6), 1389-99.
(70) Molinari, F.; Kaminska, A.; Fiermonte, G.; Boddaert, N.; Raas-Rothschild, A.; Plouin, P.; Palmieri, L.; Brunelle, F.; Palmieri, F.; Dulac, O.; Munnich, A.; Colleaux, L., Mutations in the mitochondrial glutamate carrier SLC25A22 in neonatal epileptic encephalopathy with suppression bursts. *Clin Genet* **2009,** 76, (2), 188-94.
(71) Molinari, F.; Raas-Rothschild, A.; Rio, M.; Fiermonte, G.; Encha-Razavi, F.; Palmieri, L.; Palmieri, F.; Ben-Neriah, Z.; Kadhom, N.; Vekemans, M.; Attie-Bitach, T.; Munnich, A.; Rustin, P.; Colleaux, L., Impaired mitochondrial glutamate transport in autosomal recessive neonatal myoclonic epilepsy. *Am J Hum Genet* **2005,** 76, (2), 334-9.
(72) Palmieri, F., Diseases caused by defects of mitochondrial carriers: a review. *Biochim Biophys Acta* **2008,** 1777, (7-8), 564-78.
(73) Inglis-Broadgate, S. L.; Ocaka, L.; Banerjee, R.; Gaasenbeek, M.; Chapple, J. P.; Cheetham, M. E.; Clark, B. J.; Hunt, D. M.; Halford, S., Isolation and characterization of murine Cds (CDP-diacylglycerol synthase) 1 and 2. *Gene* **2005,** 356, 19-31.
(74) Chang, J. W.; Choi, H.; Cotman, S. L.; Jung, Y. K., Lithium rescues the impaired autophagy process in CbCln3(Deltaex7/8/Deltaex7/8) cerebellar cells and reduces neuronal vulnerability to cell death via IMPase inhibition. *J Neurochem* **2011,** 116, (4), 659-68.
(75) Kimata, T.; Tanizawa, Y.; Can, Y.; Ikeda, S.; Kuhara, A.; Mori, I., Synaptic polarity depends on phosphatidylinositol signaling regulated by myo-inositol monophosphatase in Caenorhabditis elegans. *Genetics* **2012,** 191, (2), 509-21.
(76) Courilleau, D.; Chastre, E.; Sabbah, M.; Redeuilh, G.; Atfi, A.; Mester, J., B-ind1, a novel mediator of Rac1 signaling cloned from sodium butyrate-treated fibroblasts. *J Biol Chem* **2000,** 275, (23), 17344-8.
(77) Ikeda, M.; Kanao, Y.; Yamanaka, M.; Sakuraba, H.; Mizutani, Y.; Igarashi, Y.; Kihara, A., Characterization of four mammalian 3-hydroxyacyl-CoA dehydratases involved in very long-chain fatty acid synthesis. *FEBS Lett* **2008,** 582, (16), 2435-40.
(78) Vasiljevic, M.; Heisler, F. F.; Hausrat, T. J.; Fehr, S.; Milenkovic, I.; Kneussel, M.; Sieghart, W., Spatio-temporal expression analysis of the calcium-binding protein calumenin in the rodent brain. *Neuroscience* **2012,** 202, 29-41.
(79) Lyly, A.; von Schantz, C.; Heine, C.; Schmiedt, M. L.; Sipila, T.; Jalanko, A.; Kyttala, A., Novel interactions of CLN5 support molecular networking between Neuronal Ceroid Lipofuscinosis proteins. *BMC Cell Biol.* **2009,** 10, 83.

(80) Ottis, P.; Koppe, K.; Onisko, B.; Dynin, I.; Arzberger, T.; Kretzschmar, H.; Requena, J. R.; Silva, C. J.; Huston, J. P.; Korth, C., Human and rat brain lipofuscin proteome. *Proteomics* **2012,** 12, (15-16), 2445-54.
(81) Warburton, S.; Southwick, K.; Hardman, R. M.; Secrest, A. M.; Grow, R. K.; Xin, H.; Woolley, A. T.; Burton, G. F.; Thulin, C. D., Examining the proteins of functional retinal lipofuscin using proteomic analysis as a guide for understanding its origin. *Mol Vis* **2005,** 11, 1122-34.
(82) Alexeyenko, A.; Schmitt, T.; Tjarnberg, A.; Guala, D.; Frings, O.; Sonnhammer, E. L., Comparative interactomics with Funcoup 2.0. *Nucleic Acids Res* **2012,** 40, (Database issue), D821-8.
(83) Schaefer, M. H.; Fontaine, J. F.; Vinayagam, A.; Porras, P.; Wanker, E. E.; Andrade-Navarro, M. A., HIPPIE: Integrating protein interaction networks with experiment based quality scores. *PLoS ONE* **2012,** 7, (2), e31826.
(84) Tyynela, J.; Cooper, J. D.; Khan, M. N.; Shemilts, S. J.; Haltia, M., Hippocampal pathology in the human neuronal ceroid-lipofuscinoses: distinct patterns of storage deposition, neurodegeneration and glial activation. *Brain Pathol.* **2004,** 14, (4), 349-357.
(85) Oresic, K.; Mueller, B.; Tortorella, D., Cln6 mutants associated with neuronal ceroid lipofuscinosis are degraded in a proteasome-dependent manner. *Biosci Rep* **2009,** 29, (3), 173-81.
(86) Zhang, Q. C.; Petrey, D.; Deng, L.; Qiang, L.; Shi, Y.; Thu, C. A.; Bisikirska, B.; Lefebvre, C.; Accili, D.; Hunter, T.; Maniatis, T.; Califano, A.; Honig, B., Structure-based prediction of protein-protein interactions on a genome-wide scale. *Nature* **2012,** 490, (7421), 556-60.
(87) Zhang, Q. C.; Petrey, D.; Garzon, J. I.; Deng, L.; Honig, B., PrePPI: a structure-informed database of protein-protein interactions. *Nucleic Acids Res* **2013,** 41, (D1), D828-33.

FIGURE LEGENDS

Figure 1: Strategy for isolation and analysis of protein complexes in SH-SY5Y human neuroblastoma cells.

Human CLN3 / CLN5 entry clones were shuttled into NTAP or CTAP-Puro destination vectors, to generate mammalian expression vectors used to infect SH-SY5Y cells. Stably expressing clones were isolated by Flow cytometry or Puromycin selection, expanded and subjected to Tandem affinity Purification coupled to mass spectrometry (TAP-MS). CLN3 / CLN5 IP were identified and analysed by bioinformatics tools (Mascot and SAINT, respectively), prior to filtration of known contaminants. Finally, High confidence hits underwent Gene Ontology and pathway analysis to select targets for further biochemical and functional validation.

Figure 2: Generation of SH-SY5Y-NTAP-CLN3 stable cells.

(A) Immunodetection with Rabbit polyclonal anti-CLN3 (ab75959, 1:300, red) and Mouse monoclonal anti-LAMP1 [H4A3] (1:300, green), shows that CLN3 partially co-localises with the lysosomal marker, LAMP1. From top to bottom, anti-CLN3, anti-LAMP1 and overlay. Scale bar = 20 µm. Images were visualised on a Leica SP8 confocal microscope (Wetzlar, Germany). (B) Western Blot analysis of SH-SY5Y-NTAP-CLN3 stable cell lines with the CLN3 antibody, reveals two bands (at approx. 60 and 75 kDa) that were absent in either empty SH-SY5Y or SH-SY5Y-NTAP cells. Gly NTAP-CLN3 and UnGly CLN3 are abbreviations for glycosylated full-length, tagged CLN3 protein and its un-glycosylated form, respectively. Equal protein load was assessed with anti-η♯actin.

Figure 3: Validation of selected CLN3 IP in co-immunoprecipitation assays.

Co-immunoprecipitation was performed in triplicates on lysates from HEK 293 cells, transiently expressing Protein A (PA) tagged CLN3 and V5-tagged proteins of interest. Co-immunoprecipitates were resolved on 10% Tris-HCL SDS-PAGE and transferred to a nitrocellulose membrane, prior to immunodetection. Western blot analysis demonstrating the physical association between PA-CLN3 and V5-DBH (A), V5-DPM1 (B), V5-SEC61A1 (C) and V5-SLC25A10 (D). Expected molecular weight of V5-tagged constructs (in kDa): DBH-72; DPM1- 34; SEC61A1- 38; SLC25A10- 31.

Figure 4: Functional analyses of the CLN3 interactome.

(A) GO_biological process annotation of CLN3 IP by DAVID software, revealed the four most specific enriched terms: transmembrane transport; generation of precursor metabolites and energy; lipid biosynthesis process and nitrogen compound biosynthetic process (triple asterisks). 'benj' is used as an abbreviation for Benjamini-Hochberg corrected P-value. DAVID parameters of minimum count and EASE score thresholds were set at Ó 5 genes / term and 0.05, respectively. (B) Functional Cluster analysis of CLN3 IP, Cluster 2. Annotation terms are ordered based on their enrichment scores associated with the group. The most enriched GO_biological process term in Cluster 2 is transmembrane transport. CLN3 HCIP (Behrends et al., 2010) [8] recapitulated in our study and novel CLN3 IP, are shown in dark and light green, respectively. Disease proteins are boxed in orange. Functional terms (in red), associated with CLN3 are related to various categories of cellular transport, mitochondrion or organelle membranes (29 genes, Benjamini: 3.53e-14). Green represents positive association, whereas an unknown relationship is shown in black. (C) Functional Cluster analysis of CLN3 IP, Cluster 4. Positive association and unknown relationship are shown in

orange and black, respectively. Proteins enriched in Huntington's and Parkinson's disease (KEGG pathway) are shown in red. The description of functional enrichments in both clusters is provided in Supplementary Table 4B.

Figure 5: Cytoscape map of the combined CLN3-CLN5 interactome.

(A) A total of 58 CLN3 IP and 31 CLN5 IP from three independent TAP-MS experiments, are shown. Nodes (circles) represent IP and the edges (lines connecting two nodes) indicate PPI. The thickness of edges is proportional to the total spectral counts, determined by SAINT analysis. CLN3 HCIP previously determined in the autophagy network by Behrends et al. 2010 [8] and novel CLN3 IP are connected by purple and red edges, respectively. CLN3 IP verified by co-immunoprecipitation experiments are presented as diamonds with thick edges. All links to CLN5 described in this work are novel (red). Neurodegenerative disease proteins (CLN3, STRA6, TECR, DBH, PHGDH, SLC25A22, CLN5 and ATP1A3) are highlighted in orange. ARFs which are part the amyloid ß precursor protein (AßPP) interactome, as well as FKBP8 and CANX, known to have anti-apoptotic effects, are coloured blue. Proteins of the lipofuscin interactome are depicted by grey asterisks. Links to known complexes are presented as dashed lines (description in Supplementary Table 4). (B) Network view of CLN3-CLN5 functional complexes. Links to selected known protein complexes are portrayed as coloured edges. Description of known complexes is from Corum Database (Supplementary. Table 2). 139- SDH-mABC1-PIC-ANT-ATPase complex, 1183- CDC5L complex, 1442-Transporter (Ncx1)- receptor complex, 1208- Oligosaccharyltransferase OSTC-II complex, 1209-Oligosaccharyltransferase OSTC-III complex, 5206- Pentraxin complex. Var- various known complexes.

TABLES

Table 1: SAINT analysis of CLN3-IP recovered by TAP-MS.

Stable cells expressing SH-SY5Y-NTAP-CLN3 were tandem affinity purified and lysates trypsinised using standard procedures, prior to analysis by reverse phase (C18) nano-LC/ESI/MS/MS on an LTQ Orbitrap Velos (Thermos Velos) instrument. Proteins were identified with Mascot server 2.2.2 software (Matrix Sciences, www.matrix.com) against SwissProt 55.1 human database, followed by SAINT analysis and filtration of known contaminants, to generate a high confidence list of IP. Proteins with AvgP Ó 0.5 in at least two out of three experiments or Single hits of AvgP Ó 0.9 were accepted.

Table 2: SAINT analysis of CLN5-IP recovered by TAP-MS.

Stable cells expressing SH-SY5Y-CLN5-CTAP-Puro were subjected to tandem affinity purification coupled to mass spectrometry (TAP-MS) and processed similarly as indicated in Table 1.

Supplementary Figure 1: Isolation of CLN3 IP by TAP and bait recovery.

(A) Western blot analysis of the tandem affinity purified SH-SY5Y-NTAP-CLN3, showing various steps of purification. (B) Sequence coverage of identified CLN3 bait, indicating position of matched peptides in bold red. (C) Fragment ion spectra from two representative peptides (CLN3 and CDS2, left to right) detectable in the NTAP-CLN3 purified protein complex.

Supplementary Figure 2: Immunofluorescence co-localisation of CLN3 with selected IP in SH-SY5Y cells.

Human NTAP-CLN3 partially co-localises with (A) DBH, (B) DPM1, (C) SEC61A1, and (D) SLC25A10 in SH-SY5Y cells, as visualised by immunofluorescence on a Leica SP8 microscope (Wetzlar, Germany). Mouse monoclonal anti-V5 and rabbit polyclonal anti-CLN3 primary antibodies were used in combination with Alexa Fluor 488 and TRITC conjugated secondary antibodies, respectively. Images indicate anti-V5 (green, panel 1), anti-CLN3 (red, panel 2), merged staining (yellow, panel 3), co-localisation points (yellow, panel 4) and zoomed region (panel 5). The blue outline in panel 3 depicts zoomed area, shown in panel 5. Scale bar = 25µm.

Supplementary Figure 3: Generation of SH-SY5Y-CLN5-CTAP-Puro stable cells.

Western Blot analysis of SH-SY5Y-CLN5-CTAP-Puro stable cell line with anti-CLN5 and anti-Myc antibodies revealed a band at approx. 75 kDa corresponding to an un-glycosylated full length, tagged protein. The predicted size of tagged un-glycosylated CLN5 is approx. 75 kDa. A smear extending from 80-120 kDa (anti-CLN5) and 80-100 kDa (anti-Myc) is consistent with the glycosylated form of the protein. The SH-SY5Y-CTAP-Puro (empty vector) cells also show two faint nonspecific bands at 50 and 75 kDa, present in the immunodetection with anti-CLN5 but absent with the anti-Myc. Endogenous CLN5 protein is not detectable with rabbit polyclonal anti-CLN5 [C/32] [53]. The equal protein load was assessed with anti-η actin.

Supplementary Figure 4: KEGG map of interactions in Parkinson's disease.

A dynamic map of KEGG-derived interactions relevant to Parkinson's disease (PD; hsa: 05012) was constructed. Identified CLN3 IP (UQCRC2, SLC25A4, SLC25A5 and SLC25A6),

described in our study were overlaid with known PD pathway components. A direct link to synuclein (SNCA) is visible. The network was visualised in Cytoscape using Cell Region-Based Rendering And Layout (Cerebral) plug-in.

Supplementary Figure 5: Comprehensive Cytoscape map of the combined CLN3-CLN5 interactome.

A more detailed CLN3-CLN5 protein-protein interaction network comprising of known CLN3 / CLN5 IP from databases and novel ones (this study) as described in the text, was visualised using Cytoscape [51]. Nodes described in this study (yellow), those from database mining / literature (green) and involvement in neurodegenerative disease (orange), are highlighted. Disease proteins: PPT1-palmitoyl transferase 1 (CLN1), TPP1- tripeptidyl transferase 1 (CLN2), CLN6, CLN8 and SNCA- synuclein A (Parkinson's disease) are shown. The thickness of edges is proportional to the total spectral counts, determined by SAINT analysis. CLN3 HCIP previously determined in the autophagy network by Behrends et al. 2010 and novel CLN3 IP are connected by purple and red edges, respectively. CLN3 IP verified by co-immunoprecipitation experiments (this work) are shown as diamonds with thick edges and CLN5 IP described in this work are in red. Other database / literature derived links are in blue. ARFs which are part of the amyloid η♯precursor protein (AηPP) interactome, as well as FKBP8 and CANX, known to have anti-apoptotic effects, are coloured in blue. A list of all connections is given in Supplementary Table 6.

Supplementary Figure 6: Brain network analysis of CLN3-CLN5 bridging proteins.

Proteins which bridge CLN3 and CLN5 disease proteins were connected using Human Integrated Protein-Protein Interaction rEference (Hippie) database and filtered for high

expression in the brain. The medium confidence threshold (0.63 - second quartile of the HIPPIE score distribution) was used for assigning the confidence of interactions. Score ("-1") - an interaction not found in the Hippie database. PHGDH, RCN2, SLC25A4, SLC25A5, SLC25A6 can be directly connected to autophagy-linked proteins (GABARAP- Gamma-aminobutyric acid receptor-associated protein, GABARAPL1- GABA(A) receptor-associated protein like 1, GABARAPL2- GABA(A) receptor-associated protein like 2, MAP1LC3B-microtubule-associated protein 1 light chain 3 beta). CLN3 has been assigned previously to the same cellular process [8].

Supplementary Table 1A-C: Unfiltered list of proteins isolated from SH-SY5Y-NTAP-CLN3 stable cells (Exp. 1-3).

Stable cells expressing SH-SY5Y-NTAP-CLN3 were subjected to tandem affinity purification coupled to mass spectrometry (TAP-MS) and processed similarly as indicated for Table 1, except that raw data is shown without filtration steps. SAINT analysis of CLN3 baits is based on three experiments and empty NTAP vector is used as a negative control.

Supplementary Table 2: List of all CLN3 and CLN5 IP with Gene identifiers, complex attributes and OMIM phenotypes.

CLN3 / CLN5 IP were linked to NCBI Gene identifiers (Gene ID); published literature (HCIP_autophagy, Behrends et al. 2010), published mammalian protein complexes (Corum database complex attributes), lipofuscin proteome and OMIM (disease phenotypes) databases.

Supplementary Table 3: List of literature derived disease associations of CLN3-CLN5 network.

Proteins of combined CLN3 / CLN5 network were linked to literature-mined disease associations. The list of associations was derived from a database created by S. Frankild and L.J. Jensen (http://diseases.jensenlab.org/.)

Supplementary Table 4A-D: Summary list of annotations of CLN3 and CLN5 IP identified by TAP-MS.

(A) Summary list of GO_Biological Process classification and other functional terms of CLN3 IP identifed by TAP-MS. Gene ontology analysis of CLN3 IP was done by DAVID software (http://david.abcc.ncifcrf.gov/tools.jsp). The most prominent biological process terms included: transmembrane transport (GO:0055085), generation of precursor metabolites and energy (GO:0006091), lipid biosynthesis process (GO:0008610) and nitrogen compound biosynthetic process (GO:0044271). (B) Functional cluster term enrichment analysis of CLN3 IP. Using DAVID medium stringency criteria 31 clusters can be identified. (C) Functional cluster term enrichment analysis of CLN5 IP. (D) List of over-represented pathways for CLN3 and CLN5 local networks.

Supplementary Table 5A-C: Unfiltered list of proteins isolated from SH-SY5Y-CLN5-CTAP-Puro stable cells (Exp. 1-3).

Stable cells expressing SH-SY5Y-CLN5-CTAP-Puro were subjected to tandem affinity purification coupled to mass spectrometry (TAP-MS) and processed similarly as indicated for Table 1, except that raw data is shown without filtration steps. SAINT analysis of CLN5 baits is based on three experiments and empty CTAP-Puro vector is used as a negative control.

Supplementary Table 6: List of all known interactions of CLN3 and CLN5 proteins.

The combined network was compiled using interactions derived from this work, database assigned and literature published interactions.

Supplementary Table 7: Predicted functional links between CLN3-CLN5 network proteins.

CLN3 / CLN5 IP identified in TAP-MS experiments were used as input in the functional coupling analysis using FunCoup (http://FunCoup.sbc.su.se) gene / protein functional association database.

Table 1. SAINT analysis of CLN3-IP recovered by TAP-MS

Bait	Prey	Spectral[a]	Control	AvgP[b]	Comments[c]
CLN3	**IMMT**	**45, 32, 4**	**0, 0, 0**	**1**	**CLN3 HCIP_autophagy network**
CLN3	SLC25A4	74, 23, 15	0, 0, 0	1	Novel CLN3 IP
CLN3	**GCN1L1**	**40, 40, 0**	**0, 0, 0**	**1**	**CLN3 HCIP_autophagy network**
CLN3	**PRKDC**	**32, 20, 0**	**0, 0, 0**	**1**	**CLN3 HCIP_autophagy network**
CLN3	SLC25A6	82, 0, 20	0, 0, 0	0.9990	Novel CLN3 IP
CLN3	ATP2A2	13, 24, 0	0, 0, 0	0.9990	Novel CLN3 IP
CLN3	**XPO1**	**13, 18, 0**	**0, 0, 0**	**0.9980**	**CLN3 HCIP_autophagy network**
CLN3	**CPT1A**	**15, 18, 4**	**0, 0, 0**	**0.9970**	**CLN3 HCIP_autophagy network**
CLN3	SLC25A5	75, 0, 18	0, 0, 0	0.9950	Novel CLN3 IP
CLN3	SFXN3	15, 12, 3	0, 0, 0	0.9880	Novel CLN3 IP
CLN3	**HSD17B12**	**10, 13, 0**	**0, 0,0**	**0.9880**	**CLN3 HCIP_autophagy network**
CLN3	TECR	6, 10, 0	0, 0, 0	0.9850	Novel CLN3 IP
CLN3	SLC25A13	27, 25, 6	0, 0, 0	0.9820	Novel CLN3 IP
CLN3	**RPN2**	**5, 16, 0**	**0, 0, 0**	**0.9820**	**CLN3 HCIP_autophagy network**
CLN3	**PHGDH**	**18, 14, 13**	**0, 0, 0**	**0.9500**	**CLN3 HCIP_autophagy network**
CLN3	RPN1	4, 7, 0	0, 0, 0	0.9420	Novel CLN3 IP
CLN3	TMEM33	4, 8, 3	0, 0, 0	0.9310	Novel CLN3 IP
CLN3	SFXN1	10, 4, 0	0, 0, 0	0.9290	Novel CLN3 IP
CLN3	C19orf70	3, 4, 0	0, 0, 0	0.9170	Novel CLN3 IP
CLN3	SSR4	2, 9, 0	0, 0, 0	0.902	Novel CLN3 IP
CLN3	SAMM50	3, 4, 0	0, 0, 0	0.8950	Novel CLN3 IP
CLN3	CDS2	2, 5, 0	0, 0, 0	0.8910	Novel CLN3 IP
CLN3	UQCRC2	6, 3, 0	0, 0, 0	0.8820	Novel CLN3 IP
CLN3	**COX15**	**3, 4, 0**	**0, 0, 0**	**0.8770**	**CLN3 HCIP_autophagy network**
CLN3	PTPLAD1	4, 8, 4	0, 0, 0	0.8650	Novel CLN3 IP
CLN3	**SLC25A11**	**2, 5, 0**	**0, 0, 0**	**0.8530**	**CLN3 HCIP_autophagy network**
CLN3	SEC61A1	2, 5, 0	0, 0, 0	0.8480	Novel CLN3 IP
CLN3	STRA6	4, 3, 0	0, 0, 0	0.8330	Novel CLN3 IP
CLN3	**DDOST**	**2, 3, 0**	**0, 0, 0**	**0.7750**	**CLN3 HCIP_autophagy network**

Table 1. Continued

Bait	Prey	Spectral[a]	Control	AvgP[b]	Comments[c]
CLN3	SLC35B2	2, 3, 0	0, 0, 0	0.7740	Novel CLN3 IP
CLN3	SLC25A3	14, 0, 11	0, 0, 0	0.7440	Novel CLN3 IP
CLN3	EMD	4, 2, 0	0, 0, 0	0.7310	Novel CLN3 IP
CLN3	FADS2	7, 2, 0	0, 0, 0	0.7310	Novel CLN3 IP
CLN3	TFRC	2, 3, 0	0, 0, 0	0.692	Novel CLN3 IP
CLN3	CSE1L	2, 3, 0	0, 0, 0	0.603	Novel CLN3 IP
CLN3	ARF4	11	0	0.9920	Novel CLN3 IP
CLN3	DBH	8	0	0.9720	Novel CLN3 IP
CLN3	CALU	5	0	0.9680	Novel CLN3 IP
CLN3	**AUP1**	**8**	**0**	**0.9680**	**CLN3 HCIP_autophagy network**
CLN3	DPM1	6	0	0.9640	Novel CLN3 IP
CLN3	**KIAA0368**	**5**	**0**	**0.9560**	**CLN3 HCIP_autophagy network**
CLN3	XPO5	5	0	0.9560	Novel CLN3 IP
CLN3	SLC25A1	6	0	0.9500	Novel CLN3 IP
CLN3	**SLC25A22**	**6**	**0**	**0.9500**	**CLN3 HCIP_autophagy network**
CLN3	RCN2	5	0	0.9500	Novel CLN3 IP
CLN3	**SLC25A10**	**5**	**0**	**0.9480**	**CLN3 HCIP_autophagy network**
CLN3	LPHN2	6	0	0.9440	Novel CLN3 IP
CLN3	FKBP8	4	0	0.9440	Novel CLN3 IP
CLN3	ARF5	4	0	0.9420	Novel CLN3 IP
CLN3	ERLIN2	4	0	0.9340	Novel CLN3 IP
CLN3	ATP1A1	4	0	0.9320	Novel CLN3 IP
CLN3	ARF3	4	0	0.9260	Novel CLN3 IP
CLN3	SCAMP3	4	0	0.9220	Novel CLN3 IP
CLN3	**NUP205**	**5**	**0**	**0.9200**	**CLN3 HCIP_autophagy network**
CLN3	ATP5L	3	0	0.9180	Novel CLN3 IP
CLN3	FAR1	3	0	0.9120	Novel CLN3 IP

Table 1. Continued

Bait	Prey	Spectral[a]	Control	AvgP[b]	Comments[c]
CLN3	ARMC6	3	0	0.9120	Novel CLN3 IP
CLN3	LPGAT1	3	0	0.9040	Novel CLN3 IP

[a]Spectral indicates Spectral counts in each biological replicate.
[b]AvgP is the average of individual probabilities. AvgP Ó 0.5 is based on 2/3 experiments, except for single hits Ó 0.9.
[c]Novel CLN3 IP- novel interacting partner of CLN3 identified in this work.
CLN3 HCIP_autophagy network- CLN3 high confidence interacting partner, previously identified by Behrends et al. 2010, *Nature*, 2010;466(7302):68-76.

Table 2. SAINT analysis of CLN5-IP recovered by TAP-MS

Bait	Prey	Spectral[a]	Control	AvgP[b]	Comments[c]
CLN5	SEL1L	34, 12, 49	0, 0, 0	1	Novel CLN5 IP_this study
CLN5	**GANAB**	**25, 4, 52**	**0, 0, 0**	**1**	**CLN3 HCIP_autophagy network**
CLN5	SLC25A4	0, 25, 20	0, 0, 0	1	CLN3 IP_this study
CLN5	CLGN	26, 4, 58	0, 0, 0	1	Novel CLN5 IP_this study
CLN5	CANX	43, 19, 43	0, 0, 0	0.9990	Novel CLN5 IP_this study
CLN5	OS9	28, 9, 30	0, 0, 0	0.9990	Novel CLN5 IP_this study
CLN5	DBH	0, 18, 12	0, 0, 0	0.9980	CLN3 IP_this study
CLN5	SFXN3	0, 6, 13	0, 0, 0	0.9970	CLN3 IP_this study
CLN5	RCN2	0, 7, 12	0, 0, 0	0.9950	CLN3 IP_this study
CLN5	CALR	10, 0, 11	0, 0, 0	0.9880	Novel CLN5 IP_this study
CLN5	CALU	0, 5, 13	0, 0,0	0.9880	CLN3 IP_this study
CLN5	**SLC25A13**	**0, 6, 26**	**0, 0, 0**	**0.9850**	**CLN3 HCIP_autophagy network**
CLN5	ARHGAP36	5, 0, 10	0, 0, 0	0.9820	Novel CLN5 IP_this study
CLN5	**SLC25A22**	**0, 5, 8**	**0, 0, 0**	**0.9820**	**CLN3 HCIP_autophagy network**
CLN5	**SLC25A1**	**0, 2, 12**	**0, 0, 0**	**0.9500**	**CLN3 HCIP_autophagy network**
CLN5	FBXO6	4, 3, 0	0, 0, 0	0.9420	Novel CLN5 IP_this study
CLN5	FBXO27	3, 0, 4	0, 0, 0	0.9310	Novel CLN5 IP_this study
CLN5	ATP2A2	19	0	1	CLN3 IP_this study
CLN5	SLC25A5	34	0	0.9980	CLN3 IP_this study
CLN5	SLC25A6	35	0	0.9980	CLN3 IP_this study
CLN5	**PHGDH**	**5**	**0**	**0.9660**	**CLN3 HCIP_autophagy network**
CLN5	ATP1A3	8	0	0.9640	Novel CLN5 IP_this study
CLN5	ARF4	6	0	0.9580	CLN3 IP_this study
CLN5	CDIPT	6	0	0.9500	Novel CLN5 IP_this study
CLN5	SEC61A1	7	0	0.9500	CLN3 IP_this study
CLN5	HMGCS1	4	0	0.9280	Novel CLN5 IP_this study
CLN5	**XPO1**	**6**	**0**	**0.9260**	**CLN3 HCIP_autophagy network**

Table 2. Continued

Bait	Prey	Spectral[a]	Control	AvgP[b]	Comments[c]
CLN5	RPN1	6	0	0.9220	CLN3 IP_this study
CLN5	SPNS1	5	0	0.9200	Novel CLN5 IP_this study
CLN5	**SLC25A11**	**6**	**0**	**0.9120**	**CLN3 HCIP_autophagy network**
CLN5	CDS2	5	0	0.9000	CLN3 IP_this study

[a]*Sp*ectral indicates Spectral counts in each biological replicate.
[b]AvgP is the average of individual probabilities. AvgP Ó 0.5 is based on 2/3 experiments, except for single hits Ó 0.9.
[c]CLN3 IP_this study- CLN3 interacting partner identified in this work.
CLN5 IP_this study- CLN5 interacting partner identified in this work.
CLN3 HCIP_autophagy network- CLN3 high confidence interacting partner, previously identified by Behrends et al. 2010, *Nature*, 2010;466(7302):68-76.

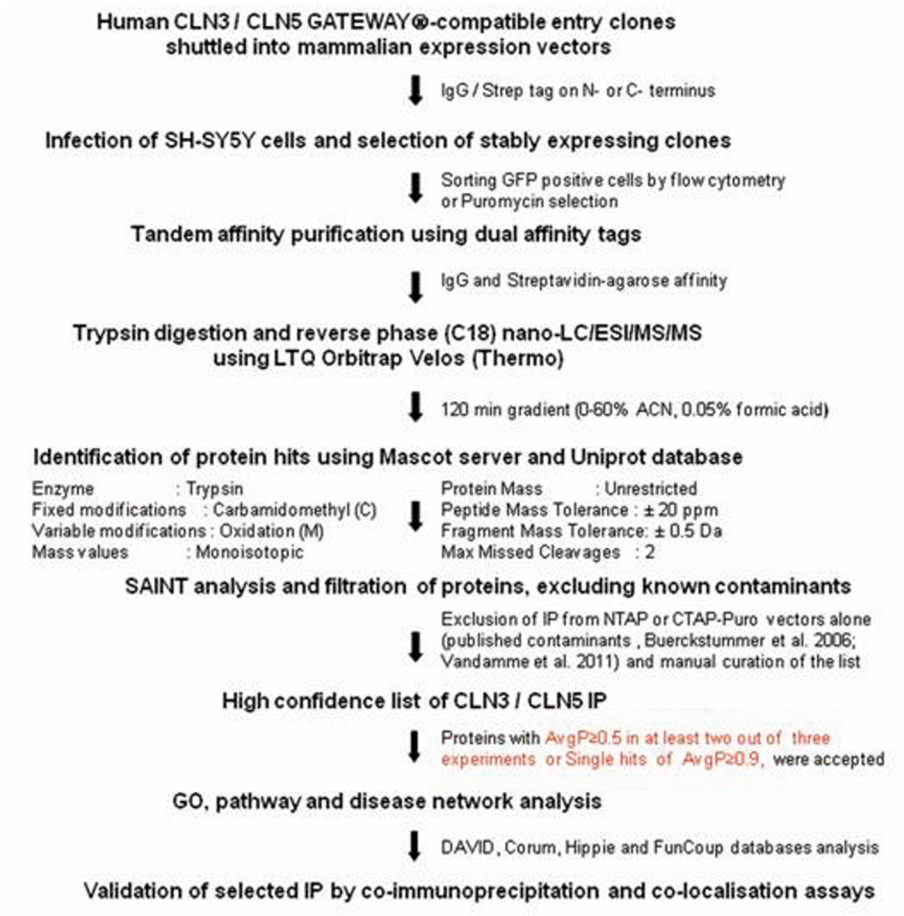

Figure 1: Strategy for isolation and analysis of protein complexes in SH-SY5Y human neuroblastoma cells. Human CLN3 / CLN5 entry clones were shuttled into NTAP or CTAP-Puro destination vectors, to generate mammalian expression vectors used to infect SH-SY5Y cells. Stably expressing clones were isolated by Flow cytometry or ¨Puromycin selection, expanded and subjected to Tandem affinity Purification coupled to mass spectrometry (TAP-MS). CLN3 / CLN5 IP were identified and analysed by bioinformatics tools (Mascot and SAINT, respectively), prior to filtration of known contaminants. Finally, High confidence hits underwent Gene Ontology and pathway analysis to select targets for further biochemical and functional validation.

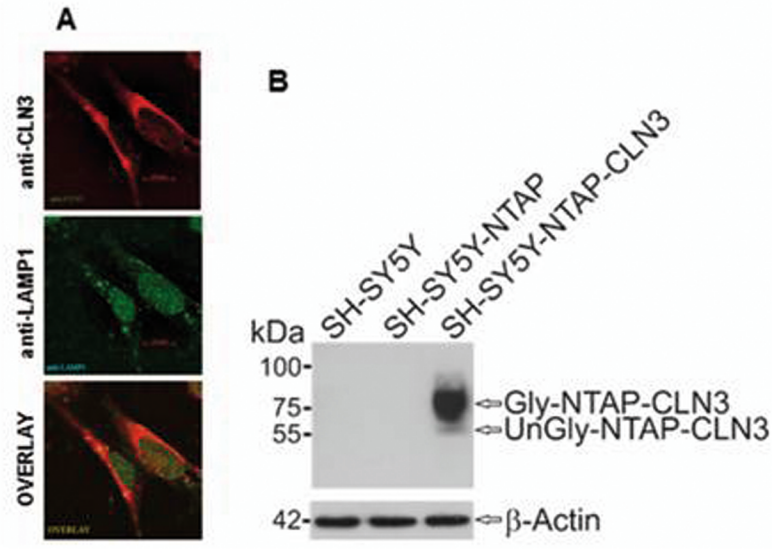

Figure 2: Generation of SH-SY5Y-NTAP-CLN3 stable cells.
(A) Immunodetection with Rabbit polyclonal anti-CLN3 (ab75959, 1:300, red) and Mouse monoclonal anti-LAMP1 [H4A3] (1:300, green), shows that CLN3 partially co-localises with the lysosomal marker, LAMP1. From top to bottom, anti-CLN3, anti-LAMP1 and overlay. Scale bar = 20 µm. Images were visualised on a LeicaSP8 confocal microscope (Wetzlar, Germany). (B) Western Blot analysis of SH-SY5Y-NTAP-CLN3 stable cell lines with the CLN3 antibody, revealstwo bands (at approx. 60 and 75 kDa) that were absent in either empty SH-SY5Y or SH-SY5Y-NTAP cells. Gly NTAP-CLN3 and UnGly CLN3 are abbreviations for glycosylated full-length, tagged CLN3 protein and its un-glycosylated form, respectively. Equal protein load was assessed with anti-b actin.

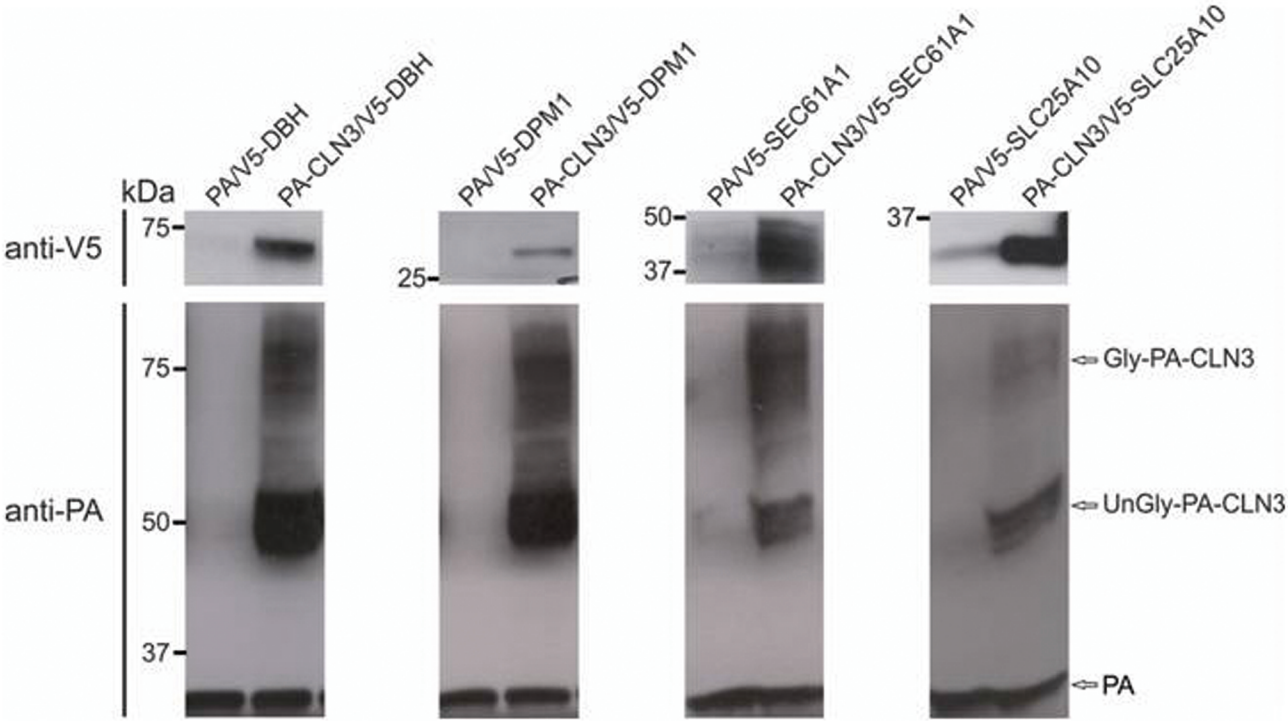

Figure 3: Validation of selected CLN3 IP in co-immunoprecipitation assays. Co-immunoprecipitation was performed in triplicates on lysates from HEK 293 cells, transiently expressing Protein A (PA) tagged CLN3 and V5-tagged proteins of interest. Co-immunoprecipitates were resolved on 10% Tris-HCL SDS-PAGE and transferred to a nitrocellulose membrane, prior to immunodetection. Western blot analysis demonstrating the physical association between PA-CLN3 and V5-DBH (A), V5-DPM1 (B), V5-SEC61A1 (C) and V5-SLC25A10 (D). Expected molecular weight of V5-tagged constructs (in kDa): DBH- 72; DPM1- 34; SEC61A1- 38; SLC25A10- 31.

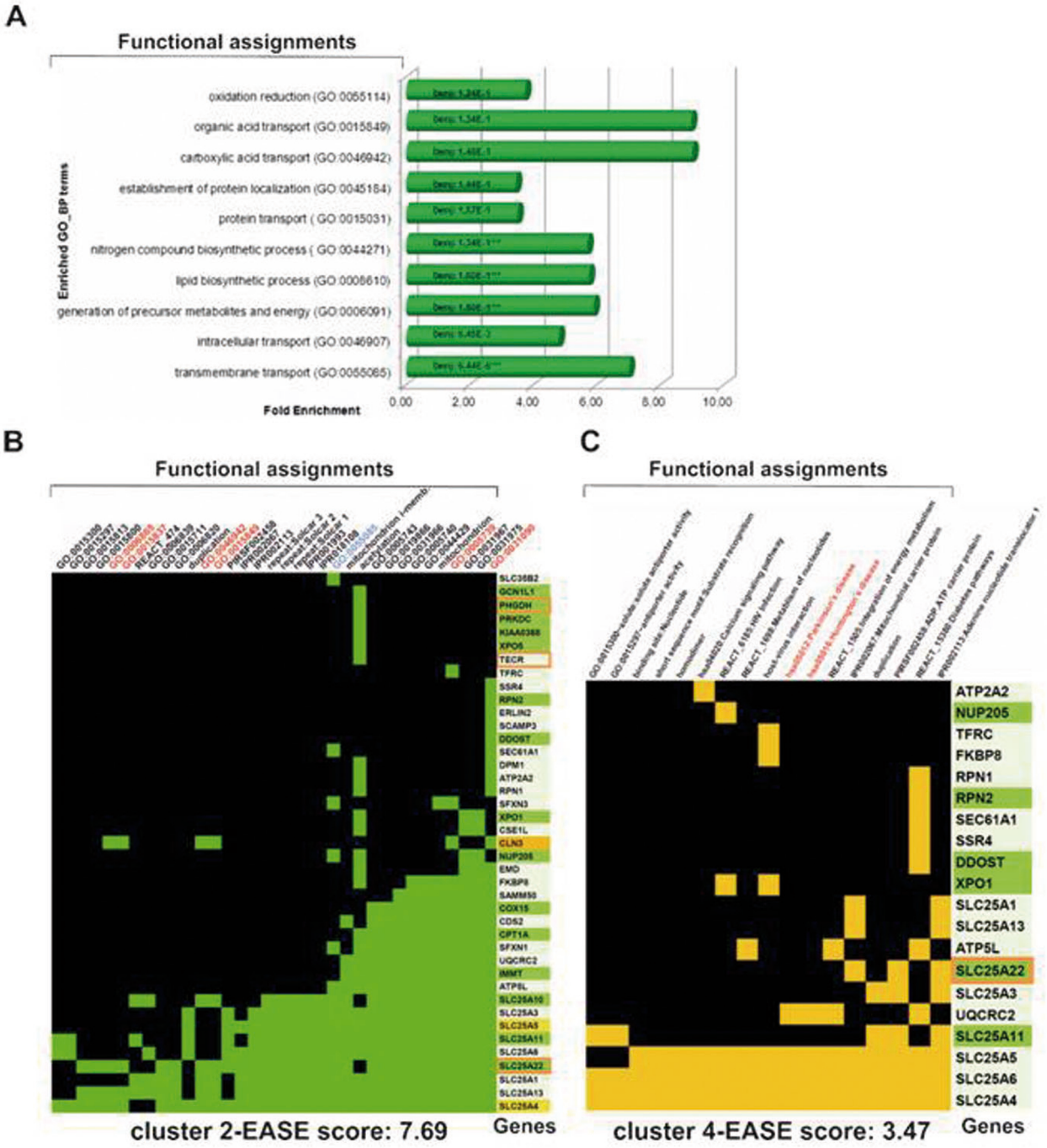

Figure 4: Functional analyses of the CLN3 interactome.
(A) GO_biological process annotation of CLN3 IP by DAVID software, revealed the four most specific enriched terms: transmembrane transport; generation of precursor metabolites and energy; lipid biosynthesis process and nitrogen compound biosynthetic process (triple asterisks). 'benj' is used as an abbreviation for Benjamini-Hochberg corrected P-value. DAVID parameters of minimum count and EASE score thresholds were set at ≥ 5 genes / term and 0.05, respectively. (B) Functional Cluster analysis of CLN3 IP, Cluster 2. Annotation terms are ordered based on their enrichment scores associated with the group. The most enriched GO_biological process term in Cluster 2 is transmembrane transport. CLN3 HCIP (Behrends et al., 2010) [8] recapitulated in our study and novel CLN3 IP, are shown in dark and light green, respectively. Disease proteins are boxed in orange. Functional terms (in red), associated with CLN3 are related to various categories of cellular transport, mitochondrion or organelle membranes (29 genes, Benjamini: 3.53e-14). Green represents positive association, whereas an unknown relationship is shown in black. (C) Functional Cluster analysis of CLN3 IP, Cluster 4. Positive association and unknown relationship are shown in orange and black, respectively. Proteins enriched in Huntington's and Parkinson's disease (KEGG pathway) are shown in red. The description of functional enrichments in both clusters is provided in Supplementary Table 4B.

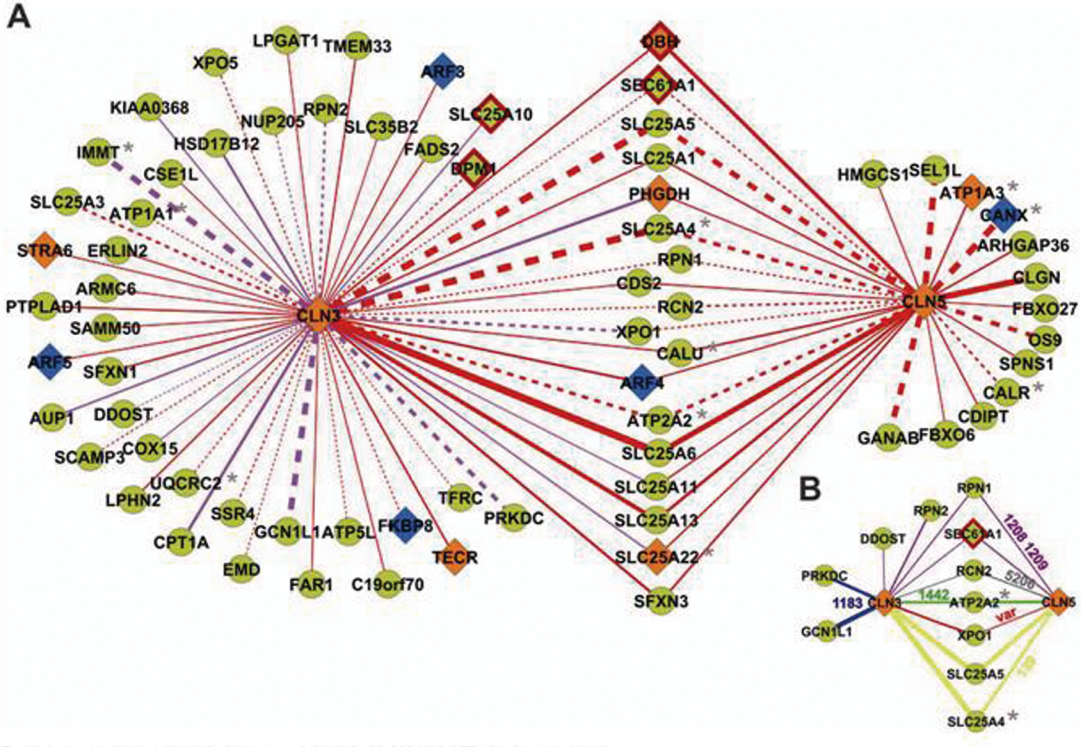

Figure 5: Cytoscape map of the combined CLN3-CLN5 interactome.
(A) A total of 58 CLN3 IP and 31 CLN5 IP from three independent TAP-MS experiments, are shown. Nodes (circles) represent IP and the edges (lines connecting two nodes) indicate PPI. The thickness of edges is proportional to the total spectral counts, determined by SAINT analysis. CLN3 HCIP previously determined in the autophagy network by Behrends et al. 2010 [8] and novel CLN3 IP are connected by purple and red edges, respectively. CLN3 IP verified by co-immunoprecipitation experiments are presented as diamonds with thick edges. All links to CLN5 described in this work are novel (red). Neurodegenerative disease proteins (CLN3, STRA6, TECR, DBH, PHGDH, SLC25A22, CLN5 and ATP1A3) are highlighted in orange. ARFs which are part the amyloid β precursor protein (AβPP) interactome, as well as FKBP8 and CANX, known to have anti-apoptotic effects, are coloured blue. Proteins of the lipofuscin interactome are depicted by grey asterisks. Links to known complexes are presented as dashed lines (description in Supplementary Table 4). (B) Network view of CLN3-CLN5 functional complexes. Links to selected known protein complexes are portrayed as coloured edges. Description of known complexes is from Corum Database (Supplementary. Table 2). 139- SDH-mABC1-PIC-ANT-ATPase complex, 1183- CDC5L complex, 1442- Transporter (Ncx1)- receptor complex, 1208- Oligosaccharyltransferase OSTC-II complex, 1209-Oligosaccharyltransferase OSTC-III complex, 5206- Pentraxin complex. Var- various known complexes.

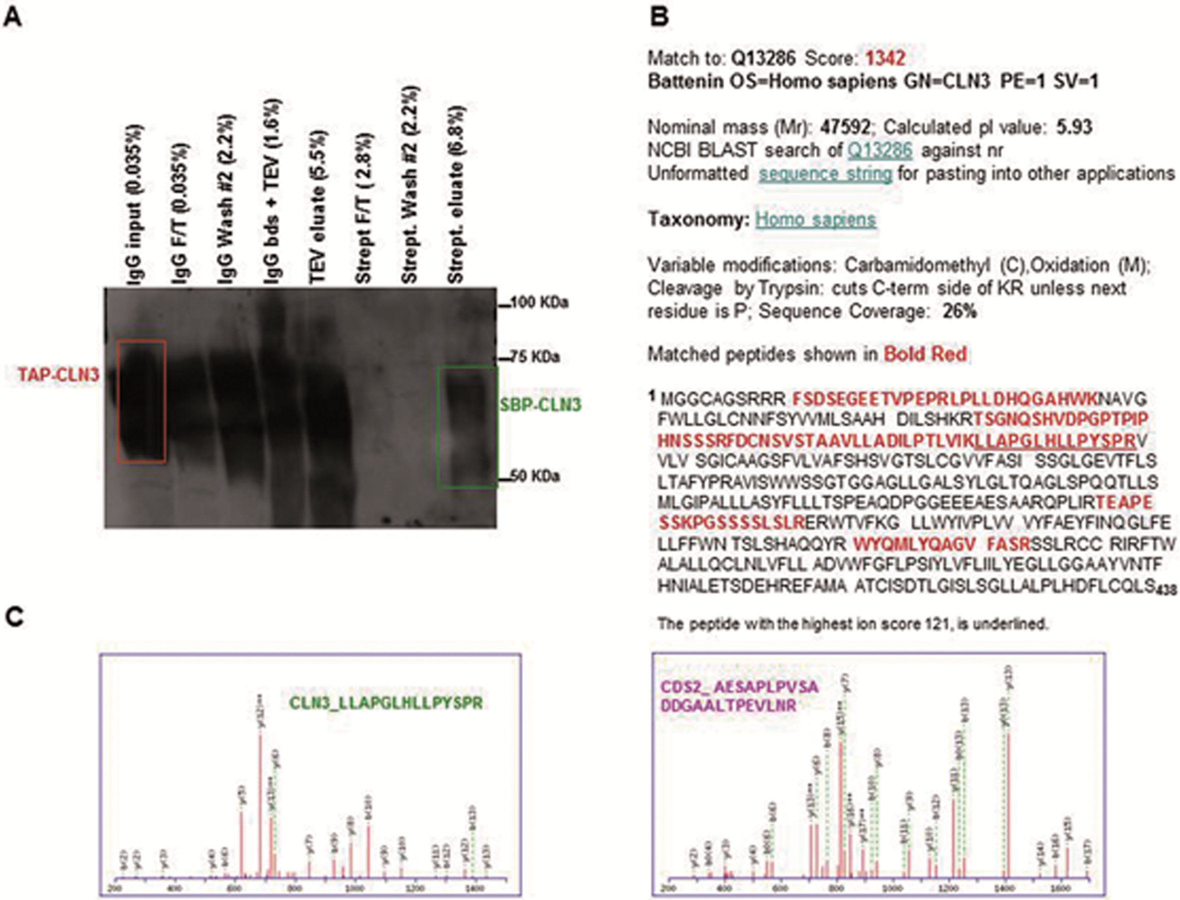

Supplementary Figure 1: Isolation of CLN3 IP by TAP and bait recovery. (A) Western blot analysis of the tandem affinity purified SH-SY5Y-NTAP-CLN3, showing various steps of purification. (B) Sequence coverage of identified CLN3 bait, indicating position of matched peptides in bold red. (C) Fragment ion spectra from two representative peptides (CLN3 and CDS2, left to right) detectable in the NTAP-CLN3 purified protein complex.

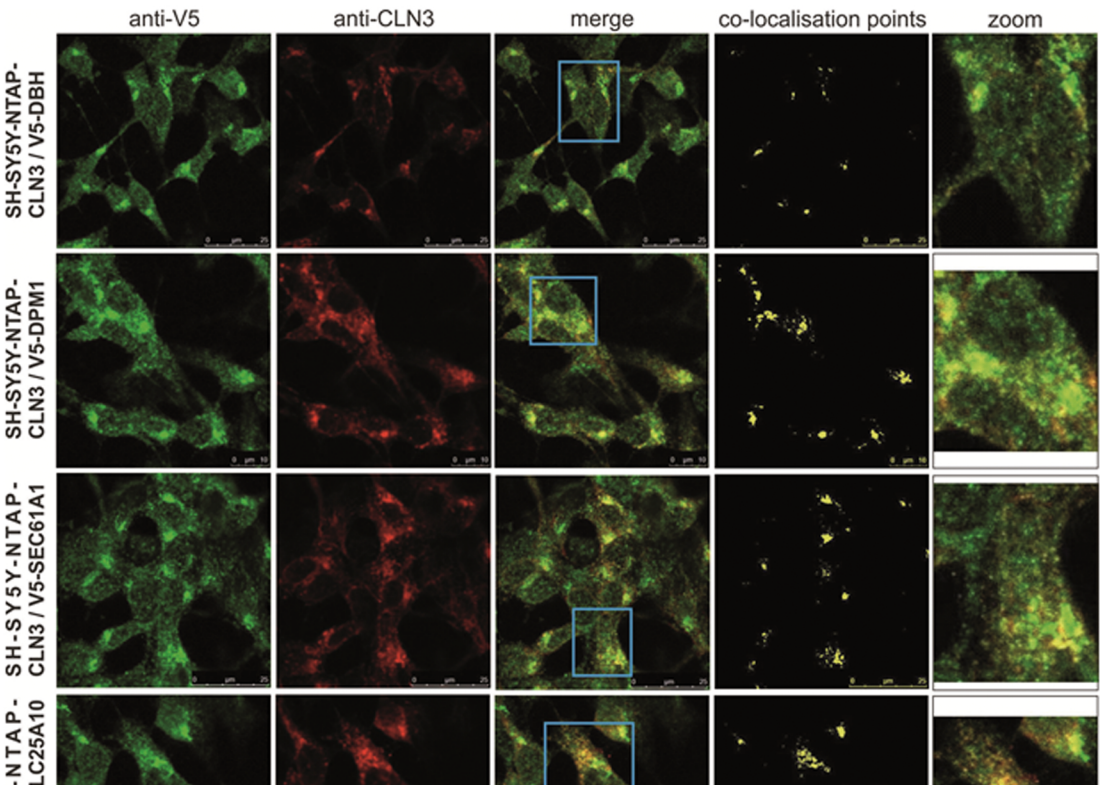

Supplementary Figure 2: Immunofluorescence co-localisation of CLN3 with selected IP in SH-SY5Y cells. Human NTAP-CLN3 partially co-localises with (A) DBH, (B) DPM1, (C) SEC61A1, and (D) SLC25A10 in SH-SY5Y cells, as visualised by immunofluorescence on a Leica SP8 microscope (Wetzlar, Germany). Mouse monoclonal anti-V5 and rabbit polyclonal anti-CLN3 primary antibodies were used in combination with Alexa Fluor 488 and TRITC conjugated secondary antibodies, respectively. Images indicate anti-V5 (green, panel 1), anti-CLN3 (red, panel 2), merged staining (yellow, panel 3), co-localisation points (yellow, panel 4) and zoomed region (panel 5). The blue outline in panel 3 depicts zoomed area, shown in panel 5. Scale bar = 25µm.

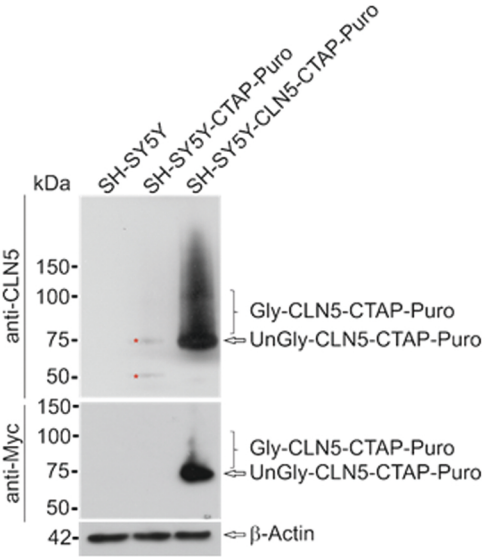

Supplementary Figure 3: Generation of SH-SY5Y-CLN5-CTAP-Puro stable cells.
Western Blot analysis of SH-SY5Y-CLN5-CTAP-Puro stable cell line with anti-CLN5 and anti- Myc antibodies revealed a band at approx. 75 kDa corresponding to an un-glycosylated full length, tagged protein. The predicted size of tagged un-glycosylated CLN5 is approx. 75 kDa. A smear extending from 80-120 kDa (anti-CLN5) and 80-100 kDa (anti-Myc) is consistent with the glycosylated form of the protein. The SH-SY5Y-CTAP-Puro (empty vector) cells also show two faint nonspecific bands at 50 and 75 kDa, present in the immunodetection with anti-CLN5 but absent with the anti-Myc. Endogenous CLN5 protein is not detectable with rabbit polyclonal anti-CLN5 [C/32] [53]. The equal protein load was assessed with anti-β actin.

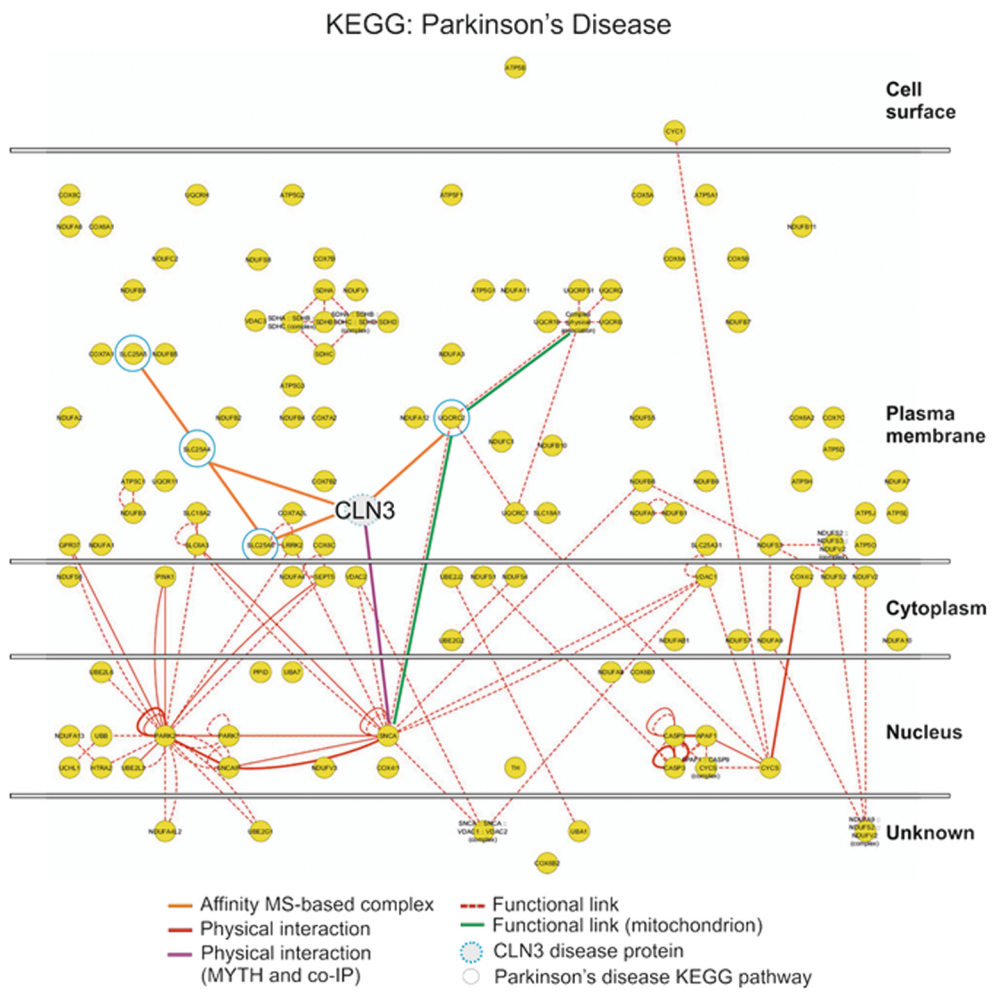

Supplementary Figure 4: KEGG map of interactions in Parkinson's disease. A dynamic map of KEGG-derived interactions relevant to Parkinson's disease (PD; hsa: 05012) was constructed. Identified CLN3 IP (UQCRC2, SLC25A4, SLC25A5 and SLC25A6), described in our study were overlaid with known PD pathway components. A direct link to synuclein (SNCA) is visible. The network was visualised in Cytoscape using Cell Region-Based Rendering And Layout (Cerebral) plug-in.

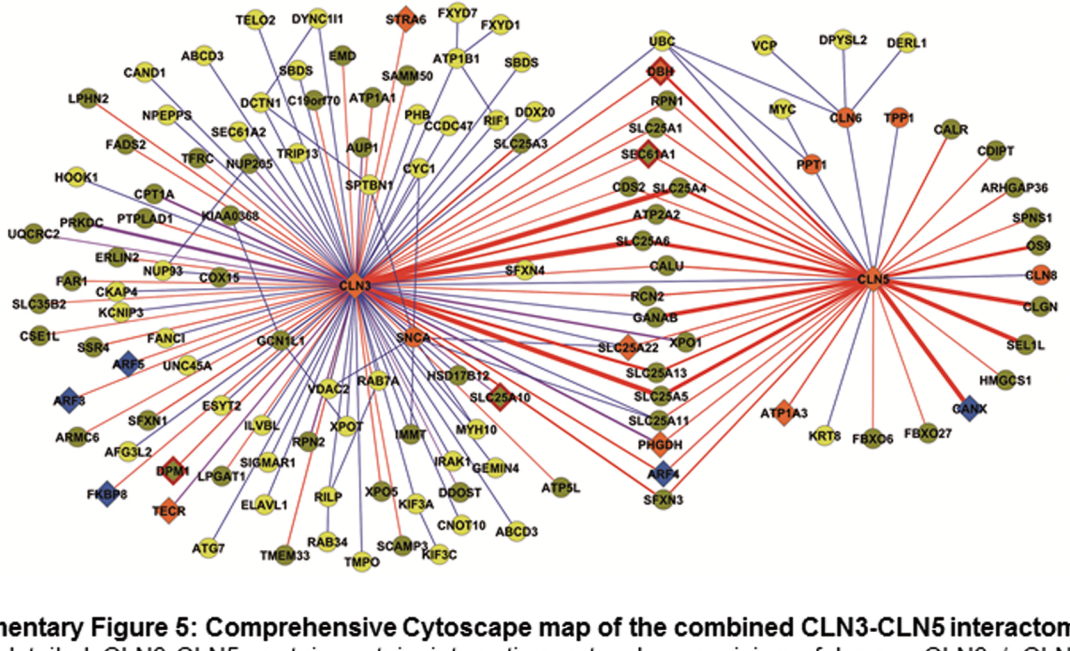

Supplementary Figure 5: Comprehensive Cytoscape map of the combined CLN3-CLN5 interactome.
A more detailed CLN3-CLN5 protein-protein interaction network comprising of known CLN3 / CLN5 IP from databases and novel ones (this study) as described in the text, was visualised using Cytoscape [51]. Nodes described in this study (yellow), those from database mining / literature (green) and involvement in neurodegenerative disease (orange), are highlighted. Disease proteins: PPT1-palmitoyl transferase 1 (CLN1), TPP1- tripeptidyl transferase 1 (CLN2), CLN6, CLN8 and SNCA- synuclein A (Parkinson's disease) are shown. The thickness of edges is proportional to the total spectral counts, determined by SAINT analysis. CLN3 HCIP previously determined in the autophagy network by Behrends et al. 2010 and novel CLN3 IP are connected by purple and red edges, respectively. CLN3 IP verified by co-immunoprecipitation experiments (this work) are shown as diamonds with thick edges and CLN5 IP described in this work are in red. Other database / literature derived links are in blue. ARFs which are part of the amyloid β precursor protein (AβPP) interactome, as well as FKBP8 and CANX, known to have anti-apoptotic effects, are coloured in blue. A list of all connections is given in Supplementary Table 6.

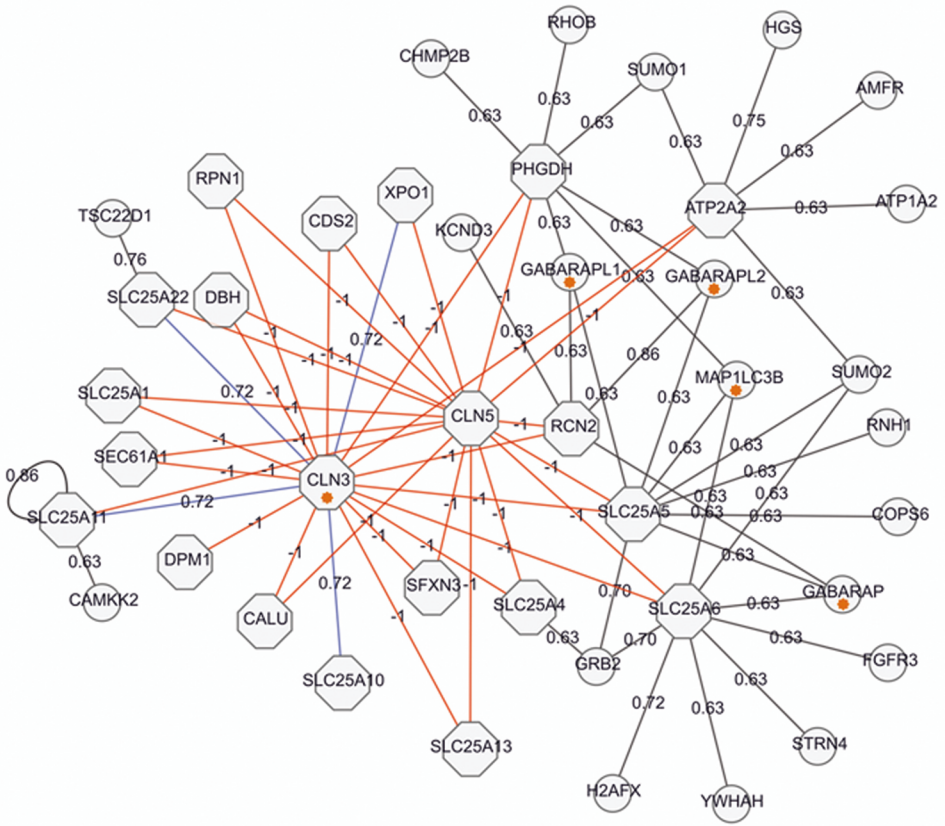

Supplementary Figure 6: Brain network analysis of CLN3-CLN5 bridging proteins.
Proteins which bridge CLN3 and CLN5 disease proteins were connected using Human Integrated Protein-Protein Interaction rEference (Hippie) database and filtered for high expression in the brain. The medium confidence threshold (0.63 - second quartile of the HIPPIE score distribution) was used for assigning the confidence of interactions. Score ("-1") - an interaction not found in the Hippie database. PHGDH, RCN2, SLC25A4, SLC25A5, SLC25A6 can be directly connected to autophagy-linked proteins (GABARAP- Gamma-aminobutyric acid receptor-associated protein, GABARAPL1- GABA(A) receptor-associated protein like 1, GABARAPL2- GABA(A) receptor-associated protein like 2, MAP1LC3B- microtubule-associated protein 1 light chain 3 beta). CLN3 has been assigned previously to the same cellular process [8].